This article has been accepted for publication in a future issue of this journal, but has not been fully edited. Content may change prior to final publication. Citation information: DOI 10.1109/ACCESS.2021.3086024, IEEE Access

IEEE Access
Multidisciplinary | Rapid Review | Open Access Journal

Date of publication xxxx 00, 0000, date of current version xxxx 00, 0000.

Digital Object Identifier 10.1109/ACCESS.2021.DOI

Adaptive-Combining-based Hybrid FSO/RF Satellite Communication With and Without HAPS

SUYASH SHAH[1], MOKKAPATI SIDDHARTH[1], NARENDRA VISHWAKARMA[1], SWAMINATHAN R[1], and AS MADHUKUMAR[2], (Senior Member, IEEE)

[1]Department of Electrical Engineering, Indian Institute of Technology Indore, India
[2]School of Computer Science and Engineering, Nanyang Technological University (NTU), Singapore

Corresponding author: Swaminathan R (e-mail: swamiramabadran@iiti.ac.in).

ABSTRACT In recent years, a growing interest has been witnessed in the usage of free space optics (FSO) link for satellite communication (SATCOM) scenarios, as it offers much higher data rates up to gigabits per second (Gbps) compared to existing radio frequency (RF) link. However, FSO links are sensitive to beam scintillation and pointing errors. In this paper, we consider a hybrid FSO/RF communication between ground station (GS) and satellite, where the RF link will act as a backup link to improve the reliability of FSO communication. In addition, we also consider high-altitude platform station (HAPS), which will act as a relay station, between GS and satellite to improve the end-to-end system performance. This has led to the development of space-air-ground integrated hybrid FSO/RF SATCOM networks. We analyse the performance of the proposed hybrid network considering an adaptive-combining-based switching scheme for both uplink and downlink scenarios with and without using HAPS as a relay station. In case of adaptive-combining-based switching scheme, the data is continuously transmitted over the FSO link, while maximal-ratio-combining (MRC) of RF and FSO links is performed when the quality of FSO link deteriorates. The performance analysis of adaptive-combining-based switching scheme in terms of outage and average symbol error rate (SER) is carried out and the same is compared with the single-link FSO SATCOM and single-threshold-based switching scheme proposed in the literature for hybrid FSO/RF SATCOM. In addition, the performance gain obtained by the proposed adaptive combining scheme over single-link FSO system for different channel conditions is also reported. Further, the asymptotic analysis is also carried out to obtain the diversity gain of the proposed system.

INDEX TERMS Adaptive combining, free space optics, high-altitude platform station (HAPS), hybrid FSO/RF, performance analysis.

I. INTRODUCTION

The advancement of space technology, together with the sophisticated space-based instruments, opened a new chapter for hybrid free space optics (FSO) / radio frequency (RF) satellite communication (SATCOM). This is also due to the increasing demand for large communication capacity and reliable communication links in SATCOM systems. A high-altitude platform station or high-altitude pseudo satellite (HAPS) is an aircraft stationed in the lower stratosphere, typically at the height of around 17 to 25 km. They act as a pseudo satellite to provide services that are generally offered by satellite. Unmanned aerial vehicle (UAV), balloons, and airships can be used as HAPS. Further, HAPS find various potential applications in disaster monitoring, agricultural observation, atmospheric observation, weather monitoring, and communication relay [1]. They can provide better coverage of smaller regions as compared to satellites. Moreover, they are easier and cheaper to deploy and maintain. HAPS, when used as a relay node [2], can improve the performance of communication between ground station (GS) and satellite. In addition, the requirement of high data rates with reliable SATCOM links for disaster monitoring, mission critical applications, etc has encouraged to propose space-air-ground integrated hybrid FSO/RF network, which is the integration of satellite system, terrestrial system, and aerial networks with both FSO and RF links [3].

This work is licensed under a Creative Commons Attribution 4.0 License. For more information, see https://creativecommons.org/licenses/by/4.0/

This article has been accepted for publication in a future issue of this journal, but has not been fully edited. Content may change prior to final publication. Citation information: DOI 10.1109/ACCESS.2021.3086024, IEEE Access

The systems used today for SATCOM have become synonymous to RF technology because of the wide-scale research, development and deployment of the RF systems. However, this large scale use of the RF systems has made the electromagnetic spectrum a scarce resource due to which most sub-bands are exclusively licensed and costly. Moreover, the electromagnetic spectrum of the RF wave is fundamentally limited in its capacity to carry the data only up to a specific rate. To cater to the needs of the advancements, we need to explore other viable communication systems which can operate in higher electromagnetic spectrum, thus having a higher data rate and opening the untouched electromagnetic spectrum to operate.

These have fostered the development of various communication technologies, one of which is optical wireless communication (OWC). OWC refers to the transmission of data in unguided propagation medium through the use of optical carriers in visible, IR and UV bands [4]. The outdoor OWC is generally referred to as FSO communication. It can tap in the otherwise untouched higher electromagnetic spectrum providing us with higher data rate up to few gigabits per second (Gbps) easily. This is a significant increase as compared to the RF link which can offer data rate only up to a few hundred megabits per seconds (Mbps). FSO uses very narrow laser beams for transmission. This spatial confinement of the FSO beam provides immunity towards electromagnetic interference, a high reuse factor and inherent security [4]. The FSO link provides a high data transfer rate for short-range transmission because of its susceptibility to different atmospheric conditions such as rain, fog and atmospheric turbulence-induced fading, which affect its reliability over the long-range transmission. In addition, pointing errors due to beam wander effect and misalignment between transmit and receive apertures also affect the the reliability of FSO communication [5]. Thus, it becomes necessary to improve the link performance of FSO communication.

The application of the FSO link in SATCOM cannot be discarded entirely because of its shortcomings. FSO finds potential applications in inter-satellite, orbit-to-GS and GS-to-orbit communication [6]. There have been various research and developments carried out by different space agencies [5], [7]. Near-Earth links have shown the potential to support high data rates greater than 1 Gbps for the space-to-ground link and 5.6 Gbps for space-to-space and ground-to-space links [8]. The lower data rate transmission in case of space-to-ground link compared to ground-to-space link is due to limited power supply availability at satellite compared to GS. Moreover, different techniques are proposed in the literature to improve the FSO link performance for SATCOM. The performance analysis of FSO-based downlink SATCOM system with spatial diversity was carried out in [9] over Gamma-Gamma turbulence induced fading channels. In [10], the bit error rate (BER) analysis of uplink SATCOM system was investigated for different modulation schemes in the presence of atmospheric turbulence and beam-wander induced pointing errors. In [11], the BER expressions for various optical modulation schemes were derived for FSO-based SATCOM systems. Moreover, aperture averaging scheme was also proposed to improve the performance of the FSO-based SATCOM system. But aperture averaging scheme helps to improve the FSO link performance only for downlink scenario and not for uplink scenario. The usage of HAPS as a relay for dual-hop FSO-based SATCOM system was proposed in [12] to overcome some of the limitations of single-hop FSO link. Further, HAPS will also play a significant role to support FSO communication due to its unique capabilities such as maneuverability, and adaptive altitude adjustment [13]. These capabilities will help them to effectively establish line-of-sight (LOS) communication links, which are essential for successful data transmission over FSO link.

The FSO and RF links are not affected by the atmospheric and weather conditions in the same way. Studies have shown that the RF link has more susceptibility towards heavy rain and oxygen absorption as compared to the FSO link and has little or no effect due to fog, turbulence, and pointing errors [14]. While in the case of FSO link, fog is seen to be the main degrading factor [4]. However, rain does not affect the reliability of FSO link significantly [4]. Moreover, this complimentary behaviour of FSO and RF links has led to the development and analysis of hybrid FSO/RF systems. These systems exploit the high data rate of FSO link. Still, they are reliable enough for long-distance communication due to backup RF link which can cater to the needs of different communication environments such as SATCOM and terrestrial communication.

One approach is to switch between the RF and FSO links (i.e. hard-switching) to use their complementary natures. However, this approach requires constant hardware switching [15], [16]. Another approach is to continuously send data over both the links and use combining techniques at the receiver [14]. But in this method, we are not using the FSO link at its highest data carrying capability because of simultaneous transmission of data over the RF link which operates at a lower data rate. Due to simultaneous transmission, the power is wasted over RF link even if the FSO link provides a good communication link. Adaptive-combining-based switching [17] provides better utilisation of FSO link. In adaptive combining scheme, FSO link is used as a primary link over which the data is transmitted continuously, while RF is used only as a backup link when the quality of FSO link deteriorates. Further, maximal-ratio-combining (MRC) of FSO and RF links is performed at the receiver when RF link is active. Recently, we investigated the outage performance of adaptive combining scheme in [18] for both terrestrial and SATCOM scenarios.

In [19], the outage performance of relaying system using low-altitude platform station (LAPS) was investigated. Here, two LAPS-based relay nodes were considered between terrestrial source and terrestrial destination nodes. Moreover, RF link was considered between LAPS and terrestrial nodes, whereas FSO link was considered between two LAPS. The performance of a multibeam satellite system was carried out

This work is licensed under a Creative Commons Attribution 4.0 License. For more information, see https://creativecommons.org/licenses/by/4.0/

This article has been accepted for publication in a future issue of this journal, but has not been fully edited. Content may change prior to final publication. Citation information: DOI 10.1109/ACCESS.2021.3086024, IEEE Access

in [20], where FSO link, which is modelled using Gamma-Gamma distribution, was assumed between GS and satellite. Further, RF link, which is modelled using shadowed-Ricean distribution, was assumed between satellite and terrestrial user nodes. In [21], outage performance and coverage probability of a downlink satellite-aerial-terrestrial system was investigated with RF transmission assuming satellite as a source node, UAV as a relay node, and a group of terrestrial receivers acting as destination nodes. In [22], outage performance of FSO communication between GS and HAPS was analyzed and the FSO link was modelled using log-normal and Gamma-Gamma distributions. Further, bit error rate (BER) performance of FSO communication using Monte-Carlo simulations between UAV and satellite was carried out in [23]. Recently, the performance of HAPS-based relaying with hybrid FSO/RF communication for SATCOM scenario assuming single-threshold-based switching scheme was investigated in [16]. In the proposed system model, both FSO and RF links, which will switch between each other using hard-switching scheme based on the channel conditions, were assumed between GS and HAPS, whereas FSO link was assumed between HAPS and satellite.

In the current work, instead of a hard-switching scheme (i.e. single-threshold-based switching scheme) proposed in [16], we assume adaptive-combining-based switching scheme between FSO and RF links and analyse the performance of single-hop and dual-hop (with HAPS) SATCOM scenarios using outage probability and average symbol error rate (SER). The RF link for SATCOM is believed to have a direct LOS component due to the presence of fewer scattering elements as compared to the terrestrial communication, where the presence of multiple scattering components is high. Ricean fading, which is having non-zero mean, models this characteristic of SATCOM RF link. While in the case of the FSO channel, the atmospheric turbulence caused by solar heating and wind leads to variations in the refractive index of the air along the transmission path. This causes random fluctuations in both the amplitude and phase of the received signal, which results in considerable degradation of the system performance. The stochastic model which is widely used to model the atmospheric turbulence-induced fading in FSO communication is the Gamma-Gamma distribution. The model also incorporates the beam-wander induced pointing errors for the uplink scenario, which can be ignored in the analysis of downlink scenario [24]. Finally, the effect of non-zero boresight pointing or misalignment errors due to misalignment between transmit and receive apertures because of mechanical vibration of HAPS and satellite is also taken into consideration in our analysis [25], [26].

A. MOTIVATIONS

The main motivations of our work are as follows:

- In prior works, the performance analysis of single-hop [9]- [11] and dual-hop (with HAPS) [12] SATCOM scenarios has been carried out by considering FSO links alone.
- In [16], performance analysis of single-hop hybrid FSO/RF SATCOM and dual-hop space-air-ground integrated hybrid FSO/RF SATCOM with HAPS has been carried for single-threshold-based hard-switching scheme, which involves frequent hardware switching with sub-optimal performance.
- In [17] and [18], adaptive-combining-based switching scheme is analysed extensively for single-hop terrestrial and SATCOM scenarios. Moreover, the closed-form expressions are derived only for the outage and not for the average symbol error rate (SER).
- There is a need to derive simpler asymptotic expressions for the system performance parameters to compute the diversity order of the system as well as to get more insights on the system performance.
- The performance analysis of adaptive-combining-based switching scheme considering hybrid FSO/RF communication for uplink and downlink scenarios has not been investigated in the literature to the best of our knowledge.

B. CONTRIBUTIONS

The major contributions of our work are as follows:

- The adaptive-combining-based switching scheme is proposed for single-hop hybrid FSO/RF SATCOM and dual-hop space-air-ground integrated hybrid FSO/RF SATCOM systems assuming both uplink and downlink scenarios. In case of dual-hop scenario, HAPS is used as a relay station between GS and low-earth orbit (LEO) satellite.
- Comprehensive performance analysis is carried out by deriving closed-form expressions for both outage and average SER by taking atmospheric turbulence, beam-wander induced pointing errors, and non-zero boresight pointing or misalignment errors into consideration. All the obtained expressions are validated using the Monte-Carlo simulation results.
- Asymptotic expressions for the performance parameters are derived to obtain useful insights on the system performance and also to obtain the diversity gain.
- To emphasis the importance of adaptive-combining-based switching scheme, its performance is compared with single-link FSO SATCOM system [10] and also with hybrid FSO/RF SATCOM system assuming single-threshold-based hard-switching scheme [16].

C. ORGANIZATION OF THE MANUSCRIPT

The manuscript is organized as follows. The detailed description about the system and channel models considered in our work is discussed in Section II. The performance analysis of the proposed system models in terms of outage and average SER is given in Section III and the asymptotic analysis is carried out in Section IV. In Section V, the numerical results and related discussions are given. Finally, concluding remarks are given in Section VI.

This work is licensed under a Creative Commons Attribution 4.0 License. For more information, see https://creativecommons.org/licenses/by/4.0/

This article has been accepted for publication in a future issue of this journal, but has not been fully edited. Content may change prior to final publication. Citation information: DOI 10.1109/ACCESS.2021.3086024, IEEE Access

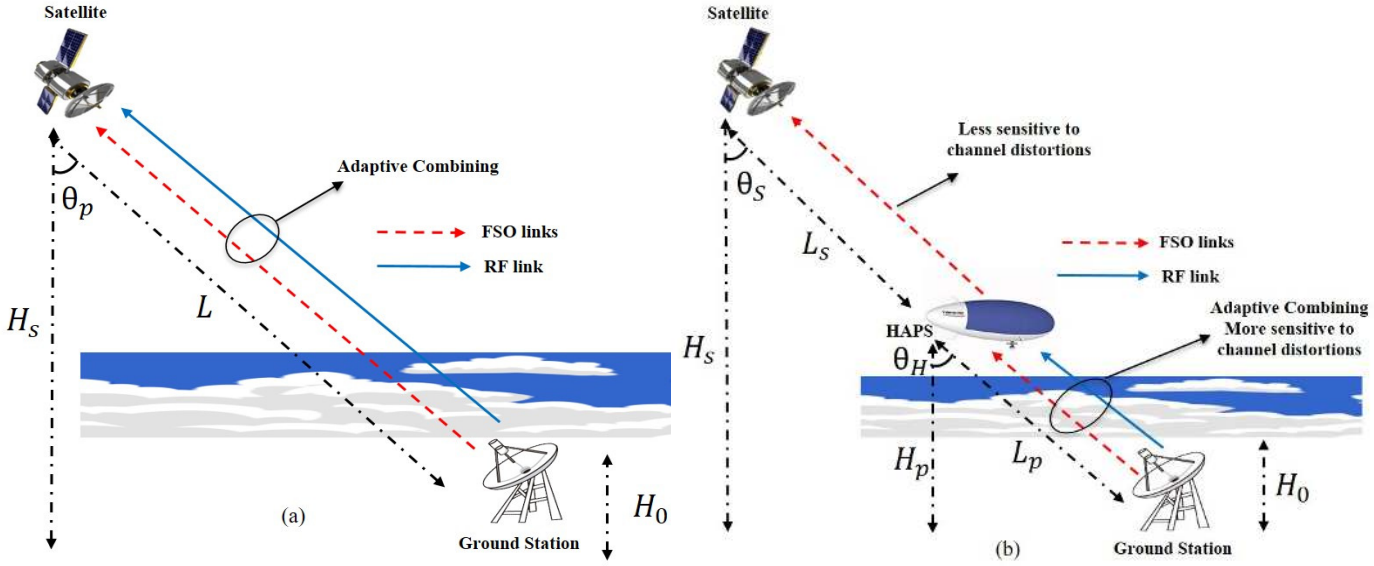

(a) Single-hop hybrid FSO/RF SATCOM **(b)** Dual-hop SAGIN-based hybrid FSO/RF SATCOM

FIGURE 1: System Models

II. SYSTEM AND CHANNEL MODELS

A. SYSTEM MODEL

In the current work, we consider two system models. Firstly, a single-hop uplink communication scenario between GS (i.e. source S) and LEO satellite (i.e. destination D) is considered as shown in Fig. 1(a). Secondly, a dual-hop uplink space-air-ground integrated network (SAGIN) scenario comprising of a GS, a HAPS-based relay node (R), and a LEO satellite as shown in Fig. 1(b) is considered. For downlink scenario, LEO satellite, HAPS, and GS will be acting as S, R, and D nodes, respectively.

In case of single-hop uplink communication, the received RF and FSO baseband signals assuming non-coherent direct detection technique for FSO signal detection at LEO satellite are, respectively, given by

$$\begin{aligned} y^r_{SD} &= \sqrt{P^r_g}\, h_{SD}\, x + n^r_{SD} \\ y^f_{SD} &= P^f_g\, R\, I_{SD}\, x + n^f_{SD}, \end{aligned} \tag{1}$$

where x is the transmitted symbol at GS, which belongs to $M-$ary phase-shift-keying (MPSK) scheme, y^r_{SD} is the received RF baseband signal at LEO satellite, y^f_{SD} is the received FSO baseband signal at LEO satellite, R is the photo-diode responsivity, P^r_g and P^f_g are the transmit RF and FSO power values at GS, h_{SD} and I_{SD} are the RF and FSO channel gains between GS and satellite, respectively, and n^r_{SD} and n^f_{SD} are the additive white Gaussian noise (AWGN) values of the RF and FSO sub-systems at satellite, respectively.

In adaptive-combining-based single-hop hybrid FSO/RF system, the signal is transmitted over FSO link, when the instantaneous signal-to-noise ratio (SNR) of the FSO sub-system at the receiver, which is denoted by γ^f_{SD}, is above a pre-determined switching threshold value γ_T. When $\gamma^f_{SD} \leq \gamma_T$, then the receiver sends a 1-bit feedback signal to activate the RF link and the signal is transmitted over both FSO and RF links, where MRC combining is performed at the receiver. The combining rule at the receiver is given by

$$y^{mrc}_{SD} = \frac{\sqrt{\gamma^r_{SD}}}{\sigma^r_{n_{SD}}} y^r_{SD} + \frac{\sqrt{\gamma^f_{SD}}}{\sigma^f_{n_{SD}}} y^f_{SD} \tag{2}$$

where γ^r_{SD} is the instantaneous of RF link, $\sigma^r_{n_{SD}}$ and $\sigma^f_{n_{SD}}$ are the standard deviation values of the AWGN of RF and FSO sub-systems, respectively. The instantaneous SNR expressions for FSO and RF links are, respectively, given by

$$\gamma^f_{SD} = \frac{(R\, P^f_g\ I_{SD})^2}{(\sigma^f_{SD})^2} \tag{3}$$

$$\gamma^r_{SD} = \frac{P^r_g |h_{SD}|^2}{(\sigma^r_{SD})^2} \tag{4}$$

Based on the definition of adaptive combining scheme, the instantaneous SNR of the system is defined as

$$\gamma_c = \begin{cases} \gamma^f_{SD} + \gamma^r_{SD}, & \gamma^f_{SD} < \gamma_T \\ \gamma^f_{SD}, & \gamma^f_{SD} \geq \gamma_T \end{cases} \tag{5}$$

In a dual-hop uplink scenario, we add a relay between GS and LEO satellite as shown in Fig. 1(b). We use HAPS stationed at the height of around 25 Km as the relay. The addition of relay breaks the link into two parts: (i) GS-HAPS link and (ii) HAPS-LEO link. The relay uses a decode-and-forward (DF) protocol. For the case of transmission between GS and HAPS, the FSO signal is highly susceptible to the atmospheric turbulence and this makes it necessary to backup the FSO link by a reliable RF link and use adaptive combining scheme. Since optical beam has to undergo minimal

This work is licensed under a Creative Commons Attribution 4.0 License. For more information, see https://creativecommons.org/licenses/by/4.0/

This article has been accepted for publication in a future issue of this journal, but has not been fully edited. Content may change prior to final publication. Citation information: DOI 10.1109/ACCESS.2021.3086024, IEEE Access

turbulence in case of transmission between HAPS and LEO satellite, only FSO link is used in this part of communication. In our work, we consider sub-carrier intensity-modulation-based MPSK (SIM-MPSK) and direct detection (DD) techniques at transmitter and receiver, respectively, for FSO communication. In addition, the data sequence is modulated using MPSK signaling scheme in case of RF communication.

In case of dual-hop space-air-ground integrated hybrid FSO/RF uplink communication, the received RF and FSO baseband signals at HAPS are, respectively, given by

$$\begin{aligned} y_{SR}^{r} &= \sqrt{P_g^r}\, h_{SR}\, x + n_{SR}^{r} \\ y_{SR}^{f} &= P_g^f\, R\, I_{SR}\, x + n_{SR}^{f}, \end{aligned} \tag{6}$$

where h_{SR} and I_{SR} are the RF and FSO channel gains between GS and HAPS, respectively, and n_{SR}^{r} and n_{SR}^{f} denote the AWGN values of RF and FSO sub-systems at HAPS, respectively. Further, the received baseband FSO signal at satellite from HAPS is given by

$$y_{RD}^{f} = P_h^f\, R\, I_{RD}\, \hat{x} + n_{RD}^{f}, \tag{7}$$

where P_h^f denotes transmit FSO power value at HAPS, $\hat{x}$ denotes the detected symbol at HAPS, I_{RD} indicates the FSO channel gains between HAPS and satellite, and n_{RD}^{f} denotes the AWGN value of FSO sub-system at satellite. The instantaneous SNR values of FSO and RF sub-systems at HAPS, which are denoted as γ_{SR}^{f} and γ_{SR}^{r}, respectively, can be written using (3) and (4) by replacing I_{SD}, h_{SD}, σ_{SD}^{r}, and σ_{SD}^{f} with I_{SR}, h_{SR}, σ_{SR}^{r}, and σ_{SR}^{f}, respectively. Similarly, the instantaneous SNR value of HAPS-to-satellite link γ_{RD}^{f} can be written using (3) by replacing I_{SD}, σ_{SD}^{f}, and P_g^f with I_{RD}, σ_{RD}^{f}, and P_h^f, respectively.

To analyse the system performance of adaptive-combining-based switching scheme for SATCOM system, first, we need to derive the expressions for the probability density function (PDF) and cumulative distribution function (CDF) of instantaneous SNR of the RF and FSO links, which are given in the next section.

B. CHANNEL MODEL

1) RF channel modelling

In SATCOM scenario, due to the presence of a strong LOS component and weak scattered components between the transmitter and receiver, the RF signal will undergo minimal scattering and reflection from the environment due to which we model the norm of small scale fading channel coefficient of the RF channel $|h_{ii}|$ using Ricean distribution, where $ii \in \{SR, SD\}$. Ricean distribution has non-zero mean representing the presence of strong LOS component. The relation between γ_{ii}^{r} and $|h_{ii}|$ is given by

$$\gamma_{ii}^{r} = \bar{\gamma}_{ii}^{r} |h_{ii}|^2, \tag{8}$$

where $\bar{\gamma}_{ii}^{r}$ is the average SNR of the RF link.

Now using power transformation of random variables, the PDF of the instantaneous SNR of the RF link can be written as [27, Eq. (2.16)]

$$f_{\gamma_{ii}^{r}}(x) = F e^{-K} e^{-Fx} I_0(2\sqrt{KFx}), \tag{9}$$

where $I_0(\cdot)$ is the zeroth-order modified Bessel function of the first kind, K is the Ricean factor, and $F = \frac{K+1}{\bar{\gamma}_{ii}^{r}}$.

By series expansion of modified Bessel and exponential functions using [28, 8.447.1] and [28, 1.211.1], respectively, the PDF can be re-written as

$$f_{\gamma_{ii}^{r}}(x) = F e^{-K} \sum_{n=0}^{\infty} \frac{(-F)^n}{n!} \sum_{i=0}^{\infty} \frac{(KF)^i}{(i!)^2} x^{n+i} \tag{10}$$

The corresponding CDF of (10) is given by

$$F_{\gamma_{ii}^{r}}(x) = F e^{-K} \sum_{n=0}^{\infty} \frac{(-F)^n}{n!} \sum_{i=0}^{\infty} \frac{(KF)^i}{(i!)^2} \frac{x^{n+i+1}}{n+i+1} \tag{11}$$

2) FSO channel modeling

The effective channel gain of the FSO link includes both atmospheric turbulence and pointing errors and is defined as

$$I_{jj} = I_{jj}^{a} I_{jj}^{p}, \tag{12}$$

where I_{jj}^{a}, $jj \in \{SR, SD, RD\}$, denotes the atmospheric turbulence induced fading of FSO link and is modelled using Gamma-Gamma distribution which accounts for moderate and strong atmospheric turbulence. The PDF of atmospheric turbulence induced fading I_{jj}^{a}, which is modelled using Gamma-Gamma distribution, is given by [16, eq.(14)]

$$\begin{aligned} f_{I_{jj}^{a}}(x) = {} & \frac{2(\alpha\beta)^{\frac{\alpha+\beta}{2}} x^{\frac{\alpha+\beta}{2}-1}}{\Gamma(\alpha)\Gamma(\beta)} \\ & \times K_{\alpha-\beta}(2\sqrt{\alpha\beta x}), \quad x > 0 \end{aligned} \tag{13}$$

where α and β are the large and small scale scattering parameters [1], $G_{p,q}^{m,n}(\cdot)$ is the Meijer G-function [28, eq.(9.301)], $K_v(\cdot)$ indicates the modified Bessel function of second kind of order v [28, eq.(8.407.1)], and $\Gamma(\cdot)$ is the gamma integral function [28, eq.(8.310.1)]. The relationship between modified Bessel function and Meijer G-function is given by [29, eq.(07.34.03.0605.01)]

$$G_{0\,2}^{2\,0}\left(z \middle| \begin{matrix} - \\ b, c \end{matrix}\right) = 2 z^{\frac{b+c}{2}} K_{b-c}(2\sqrt{z}) \tag{14}$$

Now by representing modified Bessel function in (13) in terms of Meijer G-function using (14), the PDF can be re-written as

$$f_{I_{jj}^{a}}(x) = \frac{2x^{-1}}{\Gamma(\alpha)\Gamma(\beta)} G_{0\,2}^{2\,0}\left(\alpha\beta x \middle| \begin{matrix} - \\ \alpha, \beta \end{matrix}\right) \tag{15}$$

Also, I_{jj}^{p} denotes the non-zero boresight pointing error coefficient and is given by [25]

$$I_{jj}^{p} \approx P_0 \exp\left(-\frac{2\rho^2}{w_{L_{eq}}^2}\right), \tag{16}$$

[1] Refer to [10] and [12] for the calculation of α and β in case of uplink and downlink single-hop SATCOM scenarios, respectively. Also refer to [16] for calculation of α and β in case of dual-hop scenario.

This work is licensed under a Creative Commons Attribution 4.0 License. For more information, see https://creativecommons.org/licenses/by/4.0/

This article has been accepted for publication in a future issue of this journal, but has not been fully edited. Content may change prior to final publication. Citation information: DOI 10.1109/ACCESS.2021.3086024, IEEE Access

where $w_{L_{eq}}^2$ is the equivalent beamwidth and P_0 represents the fraction of collected power at $\rho = 0$, which are given by

$$P_0 = \text{erf}^2(\nu),\ \nu = \sqrt{\frac{\pi}{2}}\frac{r_a}{w_L},\ w_{L_{eq}}^2 = \frac{w_L^2\sqrt{\pi}\text{erf}(\nu)}{2\nu\exp(-\nu^2)}, \quad (17)$$

where r_a is the radius of aperture and w_L is the beamwidth. In (16), ρ represents the radial displacement at the receiver and is given as $\rho = \sqrt{\hat{x}^2 + \hat{y}^2}$, where $\hat{x}$ and $\hat{y}$ are the random displacements, respectively, along the horizontal and elevation axes. Further, $\hat{x}$ and $\hat{y}$ are independent Gaussian random variables with non-zero means μ_x and μ_y and variances σ_x^2 and σ_y^2, respectively, and the boresight displacement is given by $S = \sqrt{\mu_x^2 + \mu_y^2}$. Therefore, the PDF of ρ follows the Beckmann distribution, which can be written as [25, Eq. (5)]

$$f_\rho(\rho) = \frac{\rho}{2\pi\sigma_x\sigma_y} \times \int_0^{2\pi} \exp\left(\frac{(\rho\cos\omega - \mu_x)^2}{2\sigma_x^2} - \frac{(\rho\sin\omega - \mu_y)^2}{2\sigma_y^2}\right) d\omega \quad (18)$$

To find the closed form expression for the PDF of I_{jj}^p, an approximation for Beckmann distribution was proposed in [26, Eq.(10)], which is given by a modified Rayleigh distribution as

$$f_\rho(\rho) \approx \frac{\rho}{\sigma_{eq}^2}\exp\left(-\frac{\rho^2}{2\sigma_{eq}^2}\right), \quad (19)$$

where

$$\sigma_{eq}^2 = \left(\frac{3\mu_x^2\sigma_x^4 + 3\mu_y^2\sigma_y^4 + \sigma_x^6 + \sigma_y^6}{2}\right)^{1/3} \quad (20)$$

The approximation performs well if the jitter standard deviations values (σ_x, σ_y) are greater than the boresight values (μ_x, μ_y) [25]. By using the random variable transformations on (12) and (19), the PDF of I_p^{jj} is given by [25, Eq.(8)]

$$f_{I_{jj}^p}(I_p) = \frac{\xi_{eq}^2}{P_{eq}^{\xi_{eq}^2}} I_p^{\xi_{eq}^2 - 1},\ 0 \le I_p \le P_{eq} \quad (21)$$

where $P_{eq} = P_0\Delta$ and pointing error coefficient $\xi_{eq} = \frac{w_{L_{eq}}}{2\sigma_{eq}}$. Here, Δ is defined as

$$\Delta = \exp\left(\frac{1}{\xi_{eq}^2} - \frac{1}{2\xi_x^2} - \frac{1}{2\xi_y^2} - \frac{\mu_x^2}{2\xi_x^2\sigma_x^2} - \frac{\mu_y^2}{2\xi_y^2\sigma_y^2}\right) \quad (22)$$

where $\xi_x = \frac{w_{L_{eq}}}{2\sigma_x}$ and $\xi_y = \frac{w_{L_{eq}}}{2\sigma_y}$. Further, by substituting $\mu_x = \mu_y = 0$, $\sigma_x = \sigma_y = \sigma_S = \sigma_{eq}$, $\Delta = 1$, and $P_{eq} = P_0$ in (20) and (21), the special case of zero boresight pointing errors is obtained [16].

The PDF of combined channel state of FSO link $I_{jj} = I_{ij}^a I_{ij}^p$ can be written as [26, Eq.(11)]

$$f_{I_{jj}}(I) = \int_{I/P_{eq}}^{\infty} \frac{1}{x} f_{I_{jj}^p}(I/x) f_{I_{jj}^a}(x) dx \quad (23)$$

By substituting (15) and (21) in (23), the integral can be simplified using [29, eq.(07.34.21.0085.01)] and [28, eq.(9.31.5)] and the PDF of I_{jj} is given by

$$f_{I_{jj}}(I) = \frac{\zeta_{eq}^2}{I\Gamma(\alpha)\Gamma(\beta)} G_{1\ 3}^{3\ 0}\left(\frac{\alpha\beta I}{P_{eq}}\middle|\begin{matrix}\xi_{eq}^2+1\\ \xi_{eq}^2, \alpha, \beta\end{matrix}\right) \quad (24)$$

The relation between the instantaneous SNR of the FSO sub-system γ_{jj}^f and the combined channel state of the FSO link I_{jj} is given by

$$\gamma_{jj}^f = \frac{\bar{\gamma}_{jj}^f I_{jj}^2(\xi_{eq}^2+1)^2}{(P_{eq}\xi_{eq}^2)^2}, \quad (25)$$

where $\bar{\gamma}_{jj}^f = \frac{(RP_g^f)^2}{(\sigma_{jj}^f)^2}\left[\frac{(P_{eq}\xi_{eq}^2)^2}{(\xi_{eq}^2+1)^2}\right]$ is the average electrical SNR of the FSO link. Now using power transformation of random variables, we get the PDF of γ_{jj}^f as

$$f_{\gamma_{jj}^f}(x) = \frac{\xi_{eq}^2 x^{-1}}{2\Gamma(\alpha)\Gamma(\beta)} G_{1,3}^{3,0}\left(Dx^{\frac{1}{2}} \mid \begin{matrix}\mathcal{B}_1\\ \mathcal{B}_2\end{matrix}\right), \quad (26)$$

where $\mathcal{B}_1 = [\mathcal{B}_{1,1}] = [\xi_{eq}^2 + 1]$, $\mathcal{B}_2 = [\mathcal{B}_{2,1}, \mathcal{B}_{2,2}, \mathcal{B}_{2,3}] = [\xi_{eq}^2, \alpha, \beta]$, and $D = \frac{\alpha\beta\xi_{eq}^2}{\xi_{eq}^2+1}(\bar{\gamma}_{jj}^f)^{-1/2}$. The CDF of (26) can be obtained as

$$F_{\gamma_{jj}^f}(x) = \frac{2^{\alpha+\beta-3}\xi_{eq}^2}{\pi\Gamma(\alpha)\Gamma(\beta)} G_{3,7}^{6,1}\left(\frac{D^2x}{16} \mid \begin{matrix}\mathcal{B}_3\\ \mathcal{B}_4\end{matrix}\right), \quad (27)$$

where $\mathcal{B}_3 = [\mathcal{B}_{3,1}, \mathcal{B}_{3,2}, \mathcal{B}_{3,3}] = \left[1, \frac{\xi_{eq}^2+1}{2}, \frac{\xi_{eq}^2+2}{2}\right]$ and $\mathcal{B}_4 = [\mathcal{B}_{4,1}, \mathcal{B}_{4,2}, \mathcal{B}_{4,3}, \mathcal{B}_{4,4}, \mathcal{B}_{4,5}, \mathcal{B}_{4,6}, \mathcal{B}_{4,7}] = \left[\frac{\xi_{eq}^2}{2}, \frac{\xi_{eq}^2+1}{2}, \frac{\alpha}{2}, \frac{\alpha+1}{2}, \frac{\beta}{2}, \frac{\beta+1}{2}, 0\right]$.

III. PERFORMANCE ANALYSIS

In this section, the outage and average SER for single-hop and dual-hop hybrid FSO/RF SATCOM systems considering adaptive combining scheme are analysed for the uplink scenario. The closed-form expression will remain the same for both uplink and downlink scenarios. However, the difference will come only in the calculation of α and β. Hence, this analysis can be extended to downlink scenario by using the corresponding values of α and β.

A. SINGLE-HOP HYBRID FSO/RF SATCOM SYSTEM

1) Outage analysis

In this subsection, we perform the outage analysis of single-hop adaptive-combining-based hybrid FSO/RF SATCOM by determining the CDF of the output instantaneous SNR $F_{\gamma_c}(x)$ after adaptive combining. This is because, the hybrid system is said to be in outage when the output instantaneous SNR after adaptive combining γ_c falls below a pre-defined outage threshold SNR γ_{out}, which can be expressed as $P_{AC} = \Pr(\gamma_c < \gamma_{out}) = F_{\gamma_c}(\gamma_{out})$. Thus, by determining $F_{\gamma_c}(x)$, we can compute the outage probability by evaluating the CDF of γ_c at γ_{out} or by replacing x with γ_{out}. Now

This work is licensed under a Creative Commons Attribution 4.0 License. For more information, see https://creativecommons.org/licenses/by/4.0/

This article has been accepted for publication in a future issue of this journal, but has not been fully edited. Content may change prior to final publication. Citation information: DOI 10.1109/ACCESS.2021.3086024, IEEE Access

according to the definition of the hybrid FSO/RF system with adaptive combining scheme, the CDF of γ_c can be written as

$$\begin{aligned} F_{\gamma_c}(x) =& Pr[\gamma_{SD}^f \geq \gamma_T, \gamma_{SD}^f < x] + \\ & Pr[\gamma_{SD}^f < \gamma_T, \gamma_{SD}^f + \gamma_{SD}^r < x] \end{aligned} \tag{28}$$

Expanding (28), we get

$$F_{\gamma_c}(x) = \begin{cases} F_1(x), & x \leq \gamma_T. \\ F_2(x) - F_{\gamma_{SD}^f}(\gamma_T) + F_{\gamma_{SD}^f}(x), & x > \gamma_T. \end{cases} \tag{29}$$

where

$$F_1(x) = \int_0^x f_{\gamma_{SD}^f + \gamma_{SD}^r}(t)dt \tag{30}$$

and

$$F_2(x) = \int_0^{\gamma_T} f_{\gamma_{SD}^f}(t) F_{\gamma_{SD}^r}(x-t)dt \tag{31}$$

Note that $f_{\gamma_{SD}^f + \gamma_{SD}^r}(x)$ can be calculated using the fact that the FSO and RF links are statistically independent of each other, which gives us

$$f_{\gamma_{SD}^f + \gamma_{SD}^r}(x) = \int_0^x f_{\gamma_{SD}^f}(t) f_{\gamma_{SD}^r}(x-t)dt \tag{32}$$

On substituting (10) and (26) in (32) and using [29, Eq. (07.34.21.0084.01)], we get

$$\begin{aligned} f_{\gamma_{SD}^f + \gamma_{SD}^r}(x) =& \frac{2^{\alpha+\beta-3}\xi_{eq}^2 F e^{-K}}{\pi\Gamma(\alpha)\Gamma(\beta)} \sum_{n=0}^{\infty} \frac{(-F)^n}{n!} \sum_{i=0}^{\infty} \frac{(KF)^i}{(i!)^2} \\ & \times x^{n+i}\Gamma(n+i+1) G_{3,7}^{6,1}\left(\frac{D^2 x}{16} \mid \begin{matrix} \mathcal{B}_5 \\ \mathcal{B}_6 \end{matrix}\right), \end{aligned} \tag{33}$$

where $\mathcal{B}_5 = [\mathcal{B}_{5,1}, \mathcal{B}_{5,2}, \mathcal{B}_{5,3}] = \left[1, \frac{\xi_{eq}^2+1}{2}, \frac{\xi_{eq}^2+2}{2}\right]$ and $\mathcal{B}_6 = [\mathcal{B}_{6,1}, \mathcal{B}_{6,2}, \mathcal{B}_{6,3}, \mathcal{B}_{6,4}, \mathcal{B}_{6,5}, \mathcal{B}_{6,6}, \mathcal{B}_{6,7}] = \left[\frac{\xi_{eq}^2}{2}, \frac{\xi_{eq}^2+1}{2}, \frac{\alpha}{2}, \frac{\alpha+1}{2}, \frac{\beta}{2}, \frac{\beta+1}{2}, -n-i\right]$.

By substituting (33) in (30) and using [29, Eq. (07.34.21.0084.01)], we get

$$\begin{aligned} F_1(x) =& \frac{2^{\alpha+\beta-3}\xi_{eq}^2 F e^{-K}}{\pi\Gamma(\alpha)\Gamma(\beta)} \sum_{n=0}^{\infty} \frac{(-F)^n}{n!} \sum_{i=0}^{\infty} \frac{(KF)^i}{(i!)^2} \\ & \times x^{n+i+1}\Gamma(n+i+1) G_{4,8}^{6,2}\left(\frac{D^2 x}{16} \mid \begin{matrix} \mathcal{B}_7 \\ \mathcal{B}_8 \end{matrix}\right), \end{aligned} \tag{34}$$

where $\mathcal{B}_7 = [\mathcal{B}_{7,1}, \mathcal{B}_{7,2}, \mathcal{B}_{7,3}, \mathcal{B}_{7,4}] = \left[-n-i, 1, \frac{\xi_{eq}^2+1}{2}, \frac{\xi_{eq}^2+2}{2}\right]$ and $\mathcal{B}_8 = [\mathcal{B}_{8,1}, \mathcal{B}_{8,2}, \mathcal{B}_{8,3}, \mathcal{B}_{8,4}, \mathcal{B}_{8,5}, \mathcal{B}_{8,6}, \mathcal{B}_{8,7}, \mathcal{B}_{8,8}] = \left[\frac{\xi_{eq}^2}{2}, \frac{\xi_{eq}^2+1}{2}, \frac{\alpha}{2}, \frac{\alpha+1}{2}, \frac{\beta}{2}, \frac{\beta+1}{2}, -n-i, -n-i-1\right]$.

Similarly, we can calculate $F_2(x)$ by substituting (11) and (26) in (31). After applying binomial expansion and using [29, Eq. (07.34.21.0084.01)], we get

$$\begin{aligned} F_2(x) =& \frac{2^{\alpha+\beta-3}\xi_{eq}^2 F e^{-K}}{\pi\Gamma(\alpha)\Gamma(\beta)} \sum_{n=0}^{\infty} \frac{(-F)^n}{n!} \sum_{i=0}^{\infty} \frac{(KF)^i x^{n+i+1}}{(i!)^2(n+i+1)} \\ & \times \sum_{p=0}^{n+i+1} \binom{n+i+1}{p} \left(\frac{-\gamma_T}{x}\right)^p G_{3,7}^{6,1}\left(\frac{D^2\gamma_T}{16} \mid \begin{matrix} \mathcal{B}_9 \\ \mathcal{B}_{10} \end{matrix}\right), \end{aligned} \tag{35}$$

where $\mathcal{B}_9 = [\mathcal{B}_{9,1}, \mathcal{B}_{9,2}, \mathcal{B}_{9,3}] = \left[1-p, \frac{\xi_{eq}^2+1}{2}, \frac{\xi_{eq}^2+2}{2}\right]$ and $\mathcal{B}_{10} = [\mathcal{B}_{10,1}, \mathcal{B}_{10,2}, \mathcal{B}_{10,3}, \mathcal{B}_{10,4}, \mathcal{B}_{10,5}, \mathcal{B}_{10,6}, \mathcal{B}_{10,7}] = \left[\frac{\xi_{eq}^2}{2}, \frac{\xi_{eq}^2+1}{2}, \frac{\alpha}{2}, \frac{\alpha+1}{2}, \frac{\beta}{2}, \frac{\beta+1}{2}, -p\right]$. Substituting (27), (34) and (35) in (29), we obtain $F_{\gamma_c}(x)$. We can determine P_{AC} using $F_{\gamma_c}(\gamma_{out})$.

2) Average SER

The conditional symbol error rate (SER) of MPSK signaling conditioned on the instantaneous SNR of the given link x is given by [15, eq.(11)]

$$P(e|x) \approx \frac{A}{2}\text{erfc}(\sqrt{x}B), \tag{36}$$

where erfc$(\cdot)$ is the complimentary error function, $B = \sin(\frac{\pi}{M})$ and

$$A = \begin{cases} 1, & M = 2. \\ 2, & M > 2. \end{cases} \tag{37}$$

Note that (36) is an approximate expression (i.e. upper bound) for the case when modulation order $M > 2$ and is the exact expression for $M = 2$ [27, eq.(8.25)]. Using Maclaurin series expansion [28, Eq. (3.321)], $P(e|x)$ can be written as

$$P(e|x) = \frac{A}{2}\left[1 - \frac{2}{\sqrt{\pi}} \sum_{p=0}^{\infty} \frac{(-1)^p x^{\frac{(2p+1)}{2}} B^{(2p+1)}}{p!(2p+1)}\right] \tag{38}$$

and in terms of Meijer G-function [29, Eq. 06.27.26.0003.01], $P(e|x)$ is given by

$$P(e|x) = \frac{A}{2\sqrt{\pi}} G_{1,2}^{2,0}\left(B^2 x \mid \begin{matrix} 1 \\ 0, \frac{1}{2} \end{matrix}\right) \tag{39}$$

The average SER of adaptive-combining-based switching scheme for hybrid FSO/RF system can be calculated by averaging the conditional error probability over the PDF of γ_c. So we need to determine the PDF of γ_c, which is denoted by $f_{\gamma_c}(x)$, and the same can be obtained by differentiating the CDF of γ_c. On differentiating (29) with respect to x, we obtain

$$f_{\gamma_c}(x) = \begin{cases} f_{\gamma_{SD}^f + \gamma_{SD}^r}(x), & x \leq \gamma_T. \\ G(x) + f_{\gamma_{SD}^f}(x), & x > \gamma_T. \end{cases} \tag{40}$$

where

$$G(x) = \int_0^{\gamma_T} f_{\gamma_{SD}^f}(t) f_{\gamma_{SD}^r}(x-t)dt \tag{41}$$

On substituting (10) and (26) in (41), $G(x)$ can be solved using [29, Eq. (07.34.21.0084.01)] and it is given by

$$\begin{aligned} G(x) =& \frac{2^{\alpha+\beta-3}\xi_{eq}^2 F e^{-K}}{\pi\Gamma(\alpha)\Gamma(\beta)} \sum_{n=0}^{\infty} \frac{(-F)^n}{n!} \sum_{i=0}^{\infty} \frac{(KF)^i x^{n+i}}{(i!)^2} \\ & \times \sum_{l=0}^{n+i} \binom{n+i}{l} \left(\frac{-\gamma_T}{x}\right)^l G_{3,7}^{6,1}\left(\frac{D^2\gamma_T}{16} \mid \begin{matrix} \mathcal{B}_{11} \\ \mathcal{B}_{12} \end{matrix}\right), \end{aligned} \tag{42}$$

This work is licensed under a Creative Commons Attribution 4.0 License. For more information, see https://creativecommons.org/licenses/by/4.0/

This article has been accepted for publication in a future issue of this journal, but has not been fully edited. Content may change prior to final publication. Citation information: DOI 10.1109/ACCESS.2021.3086024, IEEE Access

$$I_2 = \underbrace{\int_0^{\infty} P(e|x) f_{\gamma_{SD}^f}(x)dx}_{\mathrm{H}} - \int_0^{\gamma_T} P(e|x) f_{\gamma_{SD}^f}(x)dx + I_{23} = H - \frac{A}{2} F_{\gamma_{SD}^f}(\gamma_T) + \underbrace{\frac{A}{2}\int_0^{\gamma_T} \mathrm{erf}(\sqrt{x}B) f_{\gamma_{SD}^f}(x)dx}_{\mathrm{I_{22}}} + I_{23} \quad (48)$$

where $\mathcal{B}_{11} = [\mathcal{B}_{11,1}, \mathcal{B}_{11,2}, \mathcal{B}_{11,3}] = \left[1-l, \frac{\xi_{eq}^2+1}{2}, \frac{\xi_{eq}^2+2}{2}\right]$ and $\mathcal{B}_{12} = [\mathcal{B}_{12,1}, \mathcal{B}_{12,2}, \mathcal{B}_{12,3}, \mathcal{B}_{12,4}, \mathcal{B}_{12,5}, \mathcal{B}_{12,6}, \mathcal{B}_{12,7}] = \left[\frac{\xi_{eq}^2}{2}, \frac{\xi_{eq}^2+1}{2}, \frac{\alpha}{2}, \frac{\alpha+1}{2}, \frac{\beta}{2}, \frac{\beta+1}{2}, -l\right]$.

By definition, the average SER of the system can be calculated as

$$\bar{P}_e^{AC} = \int_0^{\infty} \frac{A}{2} \mathrm{erfc}(\sqrt{x}B) f_{\gamma_c}(x)dx \quad (43)$$

By substituting (40) in (43), we get

$$\begin{aligned} \bar{P}_e^{AC} &= \underbrace{\int_0^{\gamma_T} P(e|x) f_{\gamma_{SD}^f + \gamma_{SD}^r}(x)dx}_{\mathrm{I_1}} \\ &+ \underbrace{\int_{\gamma_T}^{\infty} P(e|x)(f_{\gamma_{SD}^f}(x) + G(x))dx}_{\mathrm{I_2}} \\ &= I_1 + I_2 \end{aligned} \quad (44)$$

where

$$I_1 = \int_0^{\gamma_T} \frac{A}{2} \mathrm{erfc}(\sqrt{x}B) f_{\gamma_{SD}^f + \gamma_{SD}^r}(x)\,dx \quad (45)$$

On substituting (33), (38) and using [29, Eq. (07.34.21.0084.01)], I_1 can be written as

$$\begin{aligned} I_1 = \frac{A}{2}F_1(\gamma_T) - \frac{2^{\alpha+\beta-3}\xi_{eq}^2 A F \gamma_T^{\frac{3}{2}} e^{-K}}{\pi^{\frac{3}{2}}\Gamma(\alpha)\Gamma(\beta)} \Bigg[\sum_{n=0}^{\infty} \frac{(-F\gamma_T)^n}{n!} \\ \times \sum_{i=0}^{\infty} \frac{(KF\gamma_T)^i}{(i!)^2} \Gamma(n+i+1) \sum_{l=0}^{\infty} \frac{(-B\sqrt{\gamma_T})^{(2l+1)}}{l!(2l+1)} \\ \times G_{4,8}^{6,2}\left(\frac{D^2\gamma_T}{16} \mid \begin{matrix} \mathcal{B}_{13} \\ \mathcal{B}_{14} \end{matrix}\right)\Bigg], \end{aligned} \quad (46)$$

where $\mathcal{B}_{13} = [\mathcal{B}_{13,1}, \mathcal{B}_{13,2}, \mathcal{B}_{13,3}, \mathcal{B}_{13,4}] = \left[\frac{1}{2} - n - i - l, 1, \frac{\xi_{eq}^2+1}{2}, \frac{\xi_{eq}^2+2}{2}\right]$ and $\mathcal{B}_{14} = [\mathcal{B}_{14,1}, \mathcal{B}_{14,2}, \mathcal{B}_{14,3}, \mathcal{B}_{14,4}, \mathcal{B}_{14,5}, \mathcal{B}_{14,6}, \mathcal{B}_{14,7}, \mathcal{B}_{14,8}] = \left[\frac{\xi_{eq}^2}{2}, \frac{\xi_{eq}^2+1}{2}, \frac{\alpha}{2}, \frac{\alpha+1}{2}, \frac{\beta}{2}, \frac{\beta+1}{2}, -n-i, -n-i-l-\frac{1}{2}\right]$.

Now, I_2 can be written as

$$I_2 = \int_{\gamma_T}^{\infty} P(e|x) f_{\gamma_{SD}^f}(x)dx + \underbrace{\int_{\gamma_T}^{\infty} P(e|x) G(x)dx}_{\mathrm{I_{23}}} \quad (47)$$

It is to be noted that on directly evaluating (47), we get a form which has convergence issues. So we use the property of integral to change the limits of integration in (47) as shown in (48), where $\mathrm{erf}(\cdot)$ is the error function and H is the average SER of FSO link. After simplification using [29, Eq. 07.34.21.0011.01], H is given as

$$H = \frac{2^{\alpha+\beta-4} A \xi_{eq}^2}{\pi^{3/2}\Gamma(\alpha)\Gamma(\beta)} G_{4,7}^{6,2}\left(\left(\frac{D}{4B}\right)^2 \mid \begin{matrix} \mathcal{B}_{15} \\ \mathcal{B}_{16} \end{matrix}\right), \quad (49)$$

where $\mathcal{B}_{15} = [\mathcal{B}_{15,1}, \mathcal{B}_{15,2}, \mathcal{B}_{15,3}, \mathcal{B}_{15,4}] = \left[1, \frac{1}{2}, \frac{\xi_{eq}^2+1}{2}, \frac{\xi_{eq}^2+2}{2}\right]$ and $\mathcal{B}_{16} = [\mathcal{B}_{16,1}, \mathcal{B}_{16,2}, \mathcal{B}_{16,3}, \mathcal{B}_{16,4}, \mathcal{B}_{16,5}, \mathcal{B}_{16,6}, \mathcal{B}_{16,7}] = \left[\frac{\xi_{eq}^2}{2}, \frac{\xi_{eq}^2+1}{2}, \frac{\alpha}{2}, \frac{\alpha+1}{2}, \frac{\beta}{2}, \frac{\beta+1}{2}, 0\right]$.

Now I_{22} is evaluated by using Maclaurin series expansion of the error function and by substituting (26) in (48). After simplification using [29, Eq. (07.34.21.0084.01)], I_{22} can be written as

$$\begin{aligned} I_{22} = \frac{2^{\alpha+\beta-3}\xi_{eq}^2 A}{\pi^{3/2}\Gamma(\alpha)\Gamma(\beta)} \sum_{n=0}^{\infty} \frac{(-1)^n (B\sqrt{\gamma_T})^{2n+1}}{n!(2n+1)} \\ \times G_{3,7}^{6,1}\left(\frac{D^2\gamma_T}{16} \mid \begin{matrix} \mathcal{B}_{17} \\ \mathcal{B}_{18} \end{matrix}\right), \end{aligned} \quad (50)$$

where $\mathcal{B}_{17} = [\mathcal{B}_{17,1}, \mathcal{B}_{17,2}, \mathcal{B}_{17,3}] = \left[\frac{1}{2} - n, \frac{\xi_{eq}^2+1}{2}, \frac{\xi_{eq}^2+2}{2}\right]$ and $\mathcal{B}_{18} = [\mathcal{B}_{18,1}, \mathcal{B}_{18,2}, \mathcal{B}_{18,3}, \mathcal{B}_{18,4}, \mathcal{B}_{18,5}, \mathcal{B}_{18,6}, \mathcal{B}_{18,7}] = \left[\frac{\xi_{eq}^2}{2}, \frac{\xi_{eq}^2+1}{2}, \frac{\alpha}{2}, \frac{\alpha+1}{2}, \frac{\beta}{2}, \frac{\beta+1}{2}, -n-\frac{1}{2}\right]$.

By substituting (39), (42) in (47) and after simplification using [29, Eq. (07.34.21.0085.01)], I_{23} can be written as

$$\begin{aligned} I_{23} = \frac{2^{\alpha+\beta-4}\xi_{eq}^2 A F e^{-K}}{\pi^{\frac{3}{2}}\Gamma(\alpha)\Gamma(\beta)} \sum_{n=0}^{\infty} \frac{(-F)^n}{n!} \sum_{i=0}^{\infty} \frac{(KF)^i \gamma_T^{n+i+1}}{(i!)^2} \\ \times \sum_{p=0}^{n+i} \binom{n+i}{l} (-1)^l G_{3,7}^{6,1}\left(\frac{D^2\gamma_T}{16} \mid \begin{matrix} \mathcal{B}_{11} \\ \mathcal{B}_{12} \end{matrix}\right) \\ \times G_{3,0}^{2,3}\left(B^2\gamma_T \mid \begin{matrix} \mathcal{B}_{19} \\ \mathcal{B}_{20} \end{matrix}\right), \end{aligned} \quad (51)$$

where $\mathcal{B}_{19} = [\mathcal{B}_{19,1}, \mathcal{B}_{19,2}, \mathcal{B}_{19,3}] = [l-n-i-1, 0, \frac{1}{2}]$ and $\mathcal{B}_{20} = [\mathcal{B}_{20,1}, \mathcal{B}_{20,2}] = [1, l-n-i]$.

On substituting (27), (49), (50) and (51) in (48), we get I_2 and on substituting the value of I_2 and (46) in (44), we obtain the average SER of single-hop hybrid FSO/RF SATCOM system.

B. DUAL-HOP HYBRID FSO/RF SAGIN WITH HAPS

In this subsection, the outage and average SER for dual-hop hybrid FSO/RF SAGIN with HAPS considering adaptive-combining-based switching scheme are analysed for the uplink scenario. The closed-form expression will remain the same for both uplink and downlink scenarios. However, the difference will be in the calculation of α and β, which is given in the Appendix A. Thus, the uplink analysis can be easily extended to downlink scenario. Let α_1^{up} and β_1^{up} be the large and small scale scattering parameters for GS-to-HAPS FSO link, respectively. Similarly, let α_2^{up} and β_2^{up} denote

This work is licensed under a Creative Commons Attribution 4.0 License. For more information, see https://creativecommons.org/licenses/by/4.0/

This article has been accepted for publication in a future issue of this journal, but has not been fully edited. Content may change prior to final publication. Citation information: DOI 10.1109/ACCESS.2021.3086024, IEEE Access

the large and small scale scattering parameters of HAPS-to-satellite FSO link, respectively. While for downlink scenario, let α_1^d and β_1^d represent the small scale and large scale scattering parameters for HAPS-to-GS FSO link, respectively, and α_2^d and β_2^d be the small scale and large scale scattering parameters for satellite-to-HAPS FSO link, respectively. Further, ξ_{SR} represents the pointing error coefficient between S and R nodes. Also, ξ_{RD} indicates the pointing error coefficient between R and D nodes. Using the expressions of outage and average SER of single-hop hybrid FSO/RF SATCOM system derived in subsection III-A, we can obtain the outage and average SER expressions for dual-hop hybrid FSO/RF SAGIN with HAPS considering adaptive combining scheme.

1) Outage probability

The dual-hop hybrid FSO/RF SAGIN considering adaptive combining scheme will be in outage, if either of GS-to-HAPS link or the HAPS-to-satellite link is in outage. In other words, the system will not be in outage if both the links are not in outage. Moreover, this can be evaluated using the fact that the adaptive-combining-based hybrid FSO/RF system between GS and HAPS and the single-link FSO system between HAPS and LEO satellite are statistically independent of each other. So the probability that the dual-hop hybrid FSO/RF system is not in outage can be written as

$$Z = (1 - P_{AC})(1 - P_{FSO}), \tag{52}$$

where P_{AC} is the outage probability of single-hop hybrid FSO/RF SATCOM system with adaptive combining scheme and P_{FSO} is the outage probability of the FSO system. P_{AC} and P_{FSO} are calculated by substituting α_1^{up} and β_1^{up} in (29) and α_2^{up} and β_2^{up} in (27), respectively, instead of α and β for single-hop uplink scenario. Similarly, for the downlink scenario P_{AC} and P_{FSO} are calculated by substituting α_1^d and β_1^d in (29) and α_2^d and β_2^d in (27), respectively. So, the probability of outage of dual-hop hybrid FSO/RF SAGIN with HAPS considering adaptive combining scheme is given by

$$P_{DH} = 1 - Z. \tag{53}$$

Substituting (52) in (53), we get

$$\begin{aligned} P_{DH} &= 1 - (1 - P_{AC})(1 - P_{FSO}) \\ &= P_{AC} + P_{FSO} - P_{AC} \times P_{FSO} \qquad (54) \\ &\approx P_{AC} + P_{FSO} \qquad (55) \end{aligned}$$

In (54), the negative term can be ignored as its value is very less compared to the sum of the other two terms. On substituting the values of P_{AC} and P_{FSO} in (55), we get the outage probability.

2) Average SER

The average error probability of the dual-hop hybrid FSO/RF system is expressed as [30, Eq. 21] [2]

$$\bar{P}_e^{DH} = P_{eSR} + P_{eRD} - P_{eSR}P_{eRD}\,, \tag{56}$$

[2]Note that the final term in [30, Eq. 21] is omitted, since it will not add any significant change in the end-to-end average SER of the system

where P_{eSR} and P_{eRD} denote the average SER of GS-to-HAPS and HAPS-to-satellite links, respectively.

Now for the case of uplink scenario, $P_{eSR} = \bar{P}_e^{AC}$ and $P_{eRD} = H$. While for the downlink scenario, $P_{eSR} = H$ and $P_{eRD} = \bar{P}_e^{AC}$. On substituting the values of P_{eSR} and P_{eRD} in (56), we get

$$\bar{P}_e^{DH} = \bar{P}_e^{AC} + H - \bar{P}_e^{AC} \times H \tag{57}$$

where $\bar{P}_e^{AC}$ is the average SER of single-hop hybrid FSO/RF SATCOM system with adaptive combining scheme as discussed in subsection III-A2, which is given by (44) and H is the average SER of single-hop FSO system, which is given by (49). It is to be noted that the corresponding values of large and small scale scattering parameters should be substituted in (44) and (49) to get the average SER of dual-hop hybrid FSO/RF SAGIN with adaptive combining scheme for uplink and downlink scenarios. Further, the average electrical SNR values of GS-to-satellite RF and FSO links, which are denoted as $\bar{\gamma}_{SD}^r$ and $\bar{\gamma}_{SD}^f$ should be replaced by $\bar{\gamma}_{SR}^r$ and $\bar{\gamma}_{SR}^f$ in case of uplink scenario in $\bar{P}_e^{AC}$. In addition, $\bar{\gamma}_{SD}^f$ should be replaced by $\bar{\gamma}_{RD}^f$ in H. Similarly, in case of downlink scenario, the average SNR values of satellite-to-GS RF and FSO links should be replaced by average SNR values of satellite-to-HAPS and HAPS-to-GS links appropriately.

IV. ASYMPTOTIC ANALYSIS

The asymptotic analysis is carried out to get the diversity order of the system. At higher values of average SNR, the closed-form expressions of the performance parameters can be expressed in the form $(G_c SNR)^{-G_d}$, where G_d and G_c are the diversity gain and coding gain of the system, respectively. Here, we assume $\bar{\gamma}_{jj}^f$ tends to infinity to derive the asymptotic expressions.

It is to be noted that $\bar{\gamma}_{jj}^f$ occurs only in the denominator of the input of Meijer G-function. Thus, $\bar{\gamma}_{jj}^f \to \infty$ indicates the input of Meijer G-function tending to zero. We obtain the asymptotic expressions for outage and average SER using the expansion of Meijer G-function, when its input is zero [29, Eq. (07.34.06.0040.01)]. Hence, by comparing the asymptotic expressions with the Taylor series expansion (i.e. $\sum_{i=0}^{\infty} a_i (\bar{\gamma}_{jj}^f)^{-i}$), the diversity gain is obtained, which is the smallest value of i for which the coefficient a_i is non-zero.

A. OUTAGE PROBABILITY

1) Single-hop hybrid FSO/RF SATCOM

As $\bar{\gamma}_{jj}^f \to \infty$, $P_{AC} \to P_{AC}^{asy}$ and the asymptotic expression for outage probability for the case when $\gamma_{out} \leq \gamma_T$ using [29, Eq. (07.34.06.0040.01)] is given by

$$\begin{aligned} P_{AC}^{asy} = \frac{2^{\alpha+\beta-3}\xi_{eq}^2 F e^{-K}}{\pi\Gamma(\alpha)\Gamma(\beta)} \sum_{n=0}^{\infty} \frac{(-F)^n}{n!} \sum_{i=0}^{\infty} \frac{(KF)^i}{(i!)^2} \\ \times \gamma_{out}^{n+i+1} \Gamma(n+i+1)\mathcal{C}_1, \end{aligned} \tag{58}$$

where $\mathcal{C}_1$ is given in Appendix B.

This work is licensed under a Creative Commons Attribution 4.0 License. For more information, see https://creativecommons.org/licenses/by/4.0/

This article has been accepted for publication in a future issue of this journal, but has not been fully edited. Content may change prior to final publication. Citation information: DOI 10.1109/ACCESS.2021.3086024, IEEE Access

For the case when $\gamma_{out} > \gamma_T$, the asymptotic outage probability expression is given by

$$P_{AC}^{asy} = \frac{2^{\alpha+\beta-3}\xi_{eq}^2}{\pi\Gamma(\alpha)\Gamma(\beta)}\Bigg[\mathcal{C}_2 - \mathcal{C}_3 + C_4\Bigg\{Fe^{-K}\sum_{n=0}^{\infty}\frac{(-F)^n}{n!} \times \sum_{i=0}^{\infty}\frac{(KF)^i\gamma_{out}^{n+i+1}}{(i!)^2(n+i+1)}\sum_{p=0}^{n+i+1}\binom{n+i+1}{p}\left(\frac{-\gamma_T}{\gamma_{out}}\right)^p\Bigg\}\Bigg], \tag{59}$$

where $\mathcal{C}_2$, $\mathcal{C}_3$, and $\mathcal{C}_4$ are given in Appendix B.

2) Dual-hop hybrid FSO/RF SAGIN with HAPS

As $\bar{\gamma}_{jj}^f \to \infty$, $P_{DH} \to P_{DH}^{asy}$. Using [29, Eq. (07.34.06.0040.01)], the asymptotic outage probability expression for the case $\gamma_{out} \leq \gamma_T$ can be written as

$$\begin{aligned} P_{DH}^{asy} &= P_{AC}^{asy} + P_{FSO}^{asy} \\ &= \frac{2^{\alpha_2+\beta_2-3}\xi_{eq}^2}{\pi\Gamma(\alpha_2)\Gamma(\beta_2)}\mathcal{C}_2 + \frac{2^{\alpha_1+\beta_1-3}\xi_{eq}^2 Fe^{-K}}{\pi\Gamma(\alpha_1)\Gamma(\beta_1)}\sum_{n=0}^{\infty}\frac{(-F)^n}{n!} \\ &\quad \times \sum_{i=0}^{\infty}\frac{(KF)^i\gamma_{out}^{n+i+1}\Gamma(n+i+1)}{(i!)^2}\mathcal{C}_1\,, \end{aligned} \tag{60}$$

As α_2 and β_2 are of the order of 10^4, the first term i.e. the term involving $\mathcal{C}_2$ is ignored. So P_{DH}^{asy} is approximately equal to

$$\begin{aligned} P_{DH}^{asy} &\approx \frac{2^{\alpha_1+\beta_1-3}\xi_{eq}^2 Fe^{-K}}{\pi\Gamma(\alpha_1)\Gamma(\beta_1)}\sum_{n=0}^{\infty}\frac{(-F)^n}{n!}\sum_{i=0}^{\infty}\frac{(KF)^i}{(i!)^2} \\ &\quad \times \gamma_{out}^{n+i+1}\Gamma(n+i+1)\,\mathcal{C}_1 \end{aligned} \tag{61}$$

The expression for the asymptotic outage probability for the case when $\gamma_{out} > \gamma_T$ is given by

$$\begin{aligned} P_{DH}^{asy} &= \frac{2^{\alpha_2+\beta_2-3}\xi_{eq}^2}{\pi\Gamma(\alpha_2)\Gamma(\beta_2)}\mathcal{C}_2 + \frac{2^{\alpha_1+\beta_1-3}\xi_{eq}^2}{\pi\Gamma(\alpha_1)\Gamma(\beta_1)}\Bigg[\mathcal{C}_2 - \mathcal{C}_3 \\ &\quad + \mathcal{C}_4\Bigg\{Fe^{-K}\sum_{n=0}^{\infty}\frac{(-F)^n}{n!}\sum_{i=0}^{\infty}\frac{(KF)^i\gamma_{out}^{n+i+1}}{(i!)^2(n+i+1)} \\ &\quad \times \sum_{p=0}^{n+i+1}\binom{n+i+1}{p}\left(\frac{-\gamma_T}{\gamma_{out}}\right)^p\Bigg\}\Bigg], \end{aligned} \tag{62}$$

Here, the term involving $\mathcal{C}_2$ is ignored, as α_2 and β_2 are of the order of 10^4 and the final asymptotic expression in closed-form is given by

$$P_{DH}^{asy} \approx \frac{2^{\alpha_1+\beta_1-3}\xi_{eq}^2}{\pi\Gamma(\alpha_1)\Gamma(\beta_1)}\Bigg[\mathcal{C}_2 - \mathcal{C}_3 + \mathcal{C}_4\Bigg\{Fe^{-K}\sum_{n=0}^{\infty}\frac{(-F)^n}{n!} \times \sum_{i=0}^{\infty}\frac{(KF)^i\gamma_{out}^{n+i+1}}{(i!)^2(n+i+1)}\sum_{p=0}^{n+i+1}\binom{n+i+1}{p}\left(\frac{-\gamma_T}{\gamma_{out}}\right)^p\Bigg\}\Bigg] \tag{63}$$

B. AVERAGE SER

Similar to asymptotic outage probability expression, in this section, we derive the asymptotic SER expression for single-hop and dual-hop scenarios using [29, Eq. (07.34.06.0040.01)].

1) Single-hop hybrid FSO/RF SATCOM

We denote $\bar{P}_{e/asy}^{AC}$, I_1^{asy}, I_2^{asy}, $F_1^{asy}(\gamma_T)$, H^{asy}, $F_{\gamma_{FSO}}^{asy}(\gamma_T)$, I_{22}^{asy} and I_{23}^{asy} as the asymptotic expressions of $\bar{P}_e^{AC}$, I_1, I_2, $F_1(\gamma_T)$, H, $F_{\gamma_{FSO}}(\gamma_T)$, I_{22} and I_{23} respectively, when $\bar{\gamma}_{jj}^f \to \infty$. So, from Eq.(44), we get

$$\bar{P}_{e/asy}^{AC} = I_1^{asy} + I_2^{asy} \tag{64}$$

The detailed derivations for I_1^{asy} and I_2^{asy} are given in Appendix C.

2) Dual-hop hybrid FSO/RF SAGIN with HAPS

In case of dual-hop scenario, the small scale and large scale parameters are of the order of 10^4 for HAPS-to-LEO link. This makes the asymptotic average SER of single-link FSO communication between HAPS and LEO satellite negligible as compared to the average SER of hybrid FSO/RF communication with adaptive-combining-based switching scheme between HAPS and GS. So, the asymptotic average SER expression for dual-hop scenario becomes equal to single-hop case. The only difference will be in the calculation of small scale and large scale parameters. We consider α_1^{up} and β_1^{up} for dual-hop uplink scenario and α_1^d and β_1^d are used for dual-hop downlink scenario as mentioned earlier.

The expressions derived in sections IV-A and IV-B will help us in obtaining the diversity order of single-hop hybrid FSO/RF SATCOM system and dual-hop hybrid FSO/RF SAGIN with adaptive-combining-based switching scheme. From sections IV-A and IV-B, we can see that the asymptotic expressions are of the form $\sum(G_c\bar{\gamma}_{ii}^f)^{-G_d}$, where G_c and G_d are constants and the dominant value of G_d is $\min\{\frac{\xi_{eq}^2}{2}, \frac{\xi_{eq}^2+1}{2}, \frac{\alpha}{2}, \frac{\alpha+1}{2}, \frac{\beta}{2}, \frac{\beta+1}{2}\}$ for both the outage and average SER in the cases of single-hop and dual-hop scenarios as can be seen from the expressions of $\mathcal{C}_1$ to $\mathcal{C}_9$. So we get the diversity order of single-hop hybrid FSO/RF SATCOM system as $\min\{\frac{\xi_{eq}^2}{2}, \frac{\alpha}{2}, \frac{\beta}{2}\}$. Furthermore, the diversity order of dual-hop hybrid FSO/RF SAGIN is obtained as $\min\{\frac{\xi_{SR}^2}{2}, \frac{\alpha_1^{up}}{2}, \frac{\beta_1^{up}}{2}\}$ and $\min\{\frac{\xi_{RD}^2}{2}, \frac{\alpha_1^d}{2}, \frac{\beta_1^d}{2},\}$, respectively, for uplink and downlink scenarios. It is to be noted that the effect of beam wander induced pointing errors is incorporated in the large scale scattering parameter in case of uplink scenario. Also, it is to be noted that the diversity order of dual-hop scenario is better than single-hop scenario as $\alpha_1^{up} > \alpha$ and $\beta_1^{up} > \beta$ for uplink scenario and $\alpha_1^d > \alpha$ and $\beta_1^d > \beta$ for downlink scenario. This is mainly because, the large and small scattering parameters are inversely proportional to the propagation distance. Since for dual-hop scenario the diversity order depends on scattering parameters between HAPS and GS and also as $L > L_p$, where L is the propagation distance between GS and LEO satellite and L_p denotes the propagation distance between GS and HAPS, dual-hop scenario will have better diversity order compared to single-hop scenario.

This work is licensed under a Creative Commons Attribution 4.0 License. For more information, see https://creativecommons.org/licenses/by/4.0/

This article has been accepted for publication in a future issue of this journal, but has not been fully edited. Content may change prior to final publication. Citation information: DOI 10.1109/ACCESS.2021.3086024, IEEE Access

TABLE 1: Simulation parameters

Parameter	Value
Ricean factor (K)	1
Switching Threshold (γ_T)	5 dB, 8 dB
Outage Threshold (γ_{out})	3 dB
LEO Satellite Height (H_s)	620 km
HAPS height (H_p)	25 km
GS aperture height (H_0)	1 m
Aperture radius (r_a)	10 cm
Average RF SNR ($\bar{\gamma}_{ii}$)	10, 15 dB
Wind Speed (w)	21 m/sec
Zenith Angle (ϕ_z)	80^o
Pointing error coefficients (Uplink)	$\xi_{SR} = 5$ and $\xi_{RD} = 6$

V. NUMERICAL RESULTS AND DISCUSSIONS

In this section, we analyse the closed-form expressions derived in the earlier sections. The system parameters used for the analysis are listed in the Table 1. Unless otherwise stated, the system parameters will be the same as listed in Table 1. The truncation accuracy of summation limits (for infinite summations) involved in the outage and SER expressions are given in Table 2. Further increment in the values of n, i, and l does not affect the fifth decimal figure of the outage and average SER values. All the chosen upper limit values are applicable for both single-hop and dual-hop scenarios. Further, the asymptotic versions of the expressions also have the same upper limits. The values of beam size of transmitted beam W_0 and phase front radius of curvature of the beam at the transmitter F_0 used are 0.02 m and ∞, respectively. Moreover, for simplicity, we assume $\phi_z = \theta_p = \theta_S = \theta_H$, where θ_S and θ_H are the zenith angles that indicate the angle between the zenith and the propagation orientation from HAPS-to-satellite and GS-to-HAPS, respectively. Similarly, θ_p denotes the angle between the zenith and the propagation orientation from GS-to-satellite. As the FSO link between HAPS and satellite is not very sensitive to channel distortions, we assume $\bar{\gamma}^f_{RD} = 5 \times \bar{\gamma}^f_{SR}$ for dual-hop uplink scenario.

The main reasons for the FSO link encountering less channel distortion between HAPS and satellite can be explained as follows: The concentration profile of aerosol particles, which varies with altitude, will be large only up to 1 - 2 Km immediately above the Earth's surface [5]. Thus, the aerosols distribution will be negligible above 20 Km and the effect of aerosol is not considered between HAPS and satellite FSO link. In addition, the refractive index structure parameter C_n^2, which determines strength of turbulence in atmosphere, also varies with altitude. It is to be noted that C_n^2 remains constant for near ground horizontal link [5]. However, its value decreases with increase in altitude. Since the large and small scale scattering parameters (i.e. α and β, respectively) depend on C_n^2, their values will increase with weak turbulence (i.e. decrease in C_n^2 value) and will decrease with strong turbulence (i.e. increase in C_n^2 value). It is also to be noted that the satellite is located at an altitude of around 600 Km from HAPS. Therefore, the values of α and β for the FSO link between HAPS and satellite are very large, which are typically above 500 even for the worst-case scenario. It implies that the FSO link between HAPS and satellite undergoes very weak or negligible turbulence. Further, the severity of pointing errors, which can be caused due to atmospheric turbulence induced beam wander effect or due to misalignment between transmit and receive apertures, will also be very less. Therefore, RF link is not considered as a backup for FSO link between HAPS and satellite.

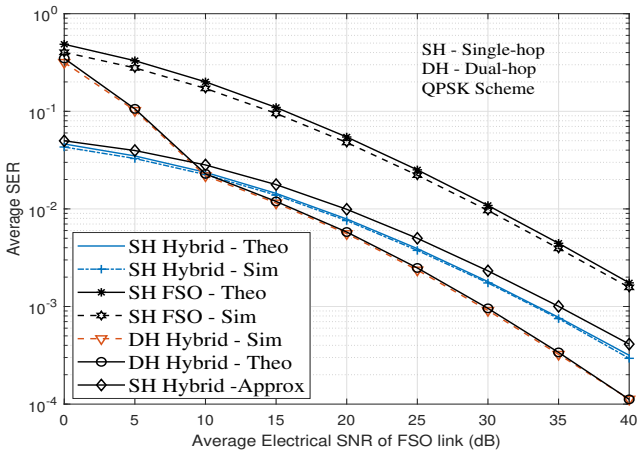

FIGURE 2: Performance comparison of theoretical and simulated average SER

Fig. 2 shows the performance comparison of theoretical and simulated average SER plots for single-hop and dual-hop scenarios. Note that the obtained average SER expressions are based on the conditional SER of MPSK signalling, which is given by (36) and the same is an approximate expression (i.e. upper bound) for the case when modulation order $M > 2$. To validate the derived upper bound average SER expression using Monte-Carlo simulations, which give exact average SER values, Fig. 2 has been included. It is observed that the theoretical SER plot is serving as an upper bound for simulation-based SER plot considering QPSK modulation scheme for single-hop FSO communication scenario. However, it is also inferred that the upper bound SER curves closely match with the simulation plots for single-hop and dual-hop hybrid FSO/RF communication scenarios based on adaptive combining. In Fig. 2, we have also plotted the average SER performance curve for single-hop hybrid scenario by truncating all the infinite summation limits to 2. It is noticed that the obtained average SER values does not agree well with the SER values obtained after truncation using the values mentioned in Table 2 as well as with the exact SER values obtained from Monte-Carlo simulations. Therefore, it is inferred that the derived analytical expressions will not match exactly with the simulation results if appropriate values for the truncation limits are not chosen.

The plots of outage and average SER are shown in Fig. 3(a) and Fig. 3(b), respectively, for uplink and downlink scenarios with respect to average electrical SNR of FSO link. The plots for uplink scenario in 3(b) are given for zenith angle value

This work is licensed under a Creative Commons Attribution 4.0 License. For more information, see https://creativecommons.org/licenses/by/4.0/

This article has been accepted for publication in a future issue of this journal, but has not been fully edited. Content may change prior to final publication. Citation information: DOI 10.1109/ACCESS.2021.3086024, IEEE Access

TABLE 2: Truncation accuracy of summation limits

Expressions	Truncation values	Final values		Chosen upper limit
		$\overline{\gamma}_{jj}^{f} = 5$	$\overline{\gamma}_{jj}^{f} = 15$	
$F_1(x)$	$n = 10,\ i = 10$	0.334481	0.148895	$n = 11,\ i = 11$
	$n = 11,\ i = 11$	0.334478	0.148894	
	$n = 12,\ i = 12$	0.334478	0.148894	
$F_2(x)$	$n = 10,\ i = 10$	0.396050	0.197460	$n = 11,\ i = 11$
	$n = 11,\ i = 11$	0.396047	0.197459	
	$n = 12,\ i = 12$	0.396048	0.197459	
I_1	$n = 9,\ i = 9,\ l = 9$	0.007323	0.003217	$n = 10,\ i = 10,\ l = 10$
	$n = 10,\ i = 10,\ l = 10$	0.007306	0.003208	
	$n = 12,\ i = 12,\ l = 12$	0.007309	0.003209	
I_{22}	$n = 10$	0.182391	0.115843	$n = 11$
	$n = 11$	0.182387	0.115840	
	$n = 12$	0.182387	0.115840	
I_{23}	$n = 4,\ i = 4$	0.000252	0.000136	$n = 5,\ i = 5$
	$n = 5,\ i = 5$	0.000249	0.000134	
	$n = 6,\ i = 6$	0.000249	0.000135	

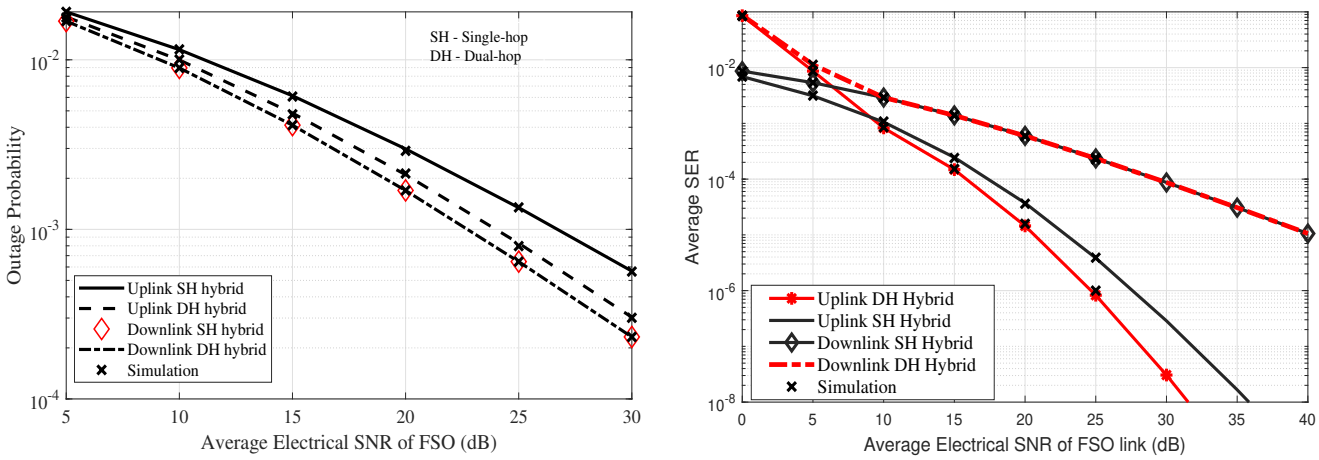

(a) Outage **(b)** Average SER

FIGURE 3: System performance parameters vs Average electrical SNR of FSO link for uplink and downlink scenarios

$\phi_z = 65°$. From Fig. 3(a), improvement in the performance is observed in case of uplink scenario for dual-hop hybrid FSO/RF SAGIN with adaptive combining scheme compared to single-hop hybrid FSO/RF SATCOM system, while there is no improvement in the performance of the dual-hop hybrid system compared to single-hop hybrid system for downlink scenario. From Fig. 3(b), it is observed that improvement in the average SER performance is observed in the uplink scenario for dual-hop hybrid system compared to single-hop hybrid system in the high-SNR region due to increase in the diversity gain value of dual-hop scenario. However, the average SER performance deteriorates to a larger extent in the low-SNR region in case of uplink scenario for dual-hop hybrid system compared to single-hop hybrid system due to degradation in the performance of HAPS-to-satellite FSO link.

In the case of downlink scenario, the data first travels in a low attenuation region during which it undergoes less attenuation. Before it reaches the high attenuation region, approximately the height at which the HAPS is stationed, it suffers low beam divergence. Due to low beam divergence, the FSO beam of single-hop system will have similar geometry as that transmitted by HAPS. Thus, no SNR gain in the system performances of dual-hop hybrid system with respect to single-hop hybrid system. While for the uplink scenario, the performance of dual-hop hybrid system is better than the single-hop system. When the beam first travels in high attenuation region, it suffers high divergence. For single-hop system, this beam continues till LEO satellite, while dual-hop system sends a new FSO signal from HAPS effectively eliminating the beam divergence and this results in the better performance of dual-hop system for the uplink. Moreover, due to the similarity in the system performances of single-hop and dual-hop hybrid FSO/RF systems with adaptive combining scheme for the case of downlink transmission, we are mainly interested in the trends of the uplink hybrid FSO/RF SATCOM system with adaptive combining scheme.

In Fig. 4, the outage performance versus switching threshold with varying average SNR of FSO link for single-hop and dual-hop hybrid FSO/RF systems are shown for the uplink scenario. For single-hop scenario, the outage performance is plotted for $\gamma_{out} = 5$ dB, while for dual-hop scenario it is

This work is licensed under a Creative Commons Attribution 4.0 License. For more information, see https://creativecommons.org/licenses/by/4.0/

This article has been accepted for publication in a future issue of this journal, but has not been fully edited. Content may change prior to final publication. Citation information: DOI 10.1109/ACCESS.2021.3086024, IEEE Access

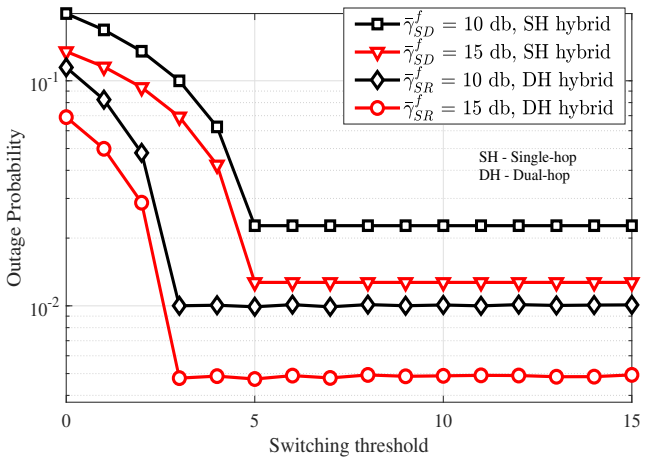

FIGURE 4: Outage probability versus threshold SNR for different values of average SNR of FSO link

plotted for $\gamma_{out} = 3$ dB. From the figure, we can observe that as the switching threshold increases, the outage probability of the system decreases and then it becomes constant. For $\gamma_T \geq \gamma_{out}$ the outage probability of the system is constant or independent of γ_T. This is mainly because, we can see from (29) that the outage probability $F_{\gamma_c}(\gamma_{out}) = F_1(\gamma_{out})$ under the condition when $\gamma_{out} \leq \gamma_T$ and the CDF $F_1(x)$ evaluated at $x = \gamma_{out}$ is independent of γ_T. The value of γ_T, for which the outage probability is minimum, does not change with average electrical SNR of FSO link. Therefore, we fix $\gamma_T \geq \gamma_{out}$ for the optimum system performance.

Fig. 5(a) shows the outage probability comparison of single-hop hard-switching-based hybrid FSO/RF SATCOM system [16], single-hop hybrid FSO/RF SATCOM system with adaptive combining scheme, single-hop RF, and single-hop FSO SATCOM systems for uplink scenario [10]. The parameters assumed in the simulations are $\gamma_T = 10$ dB and $\bar{\gamma}^r_{SD} = 5$ dB. It is to be noted that hard-switching-based hybrid FSO/RF system was proposed in [16] for SATCOM scenario, where the FSO link will be used for transmission as long as the instantaneous SNR value is above a threshold value (i.e. $\gamma^f_{SD} > \gamma_T$). When the instantaneous SNR value of FSO link is unacceptable (i.e. $\gamma^f_{SD} < \gamma_T$), then RF link will be activated for transmission and the system will be in outage if $\gamma^r_{SD} < \gamma_{out}$. From the outage plots, we can observe that the single-hop hybrid FSO/RF SATCOM system with adaptive-combining-based switching scheme assuming fixed RF SNR performs better than the single-hop FSO SATCOM system and single-hop hard-switching-based hybrid FSO/RF SATCOM system with the SNR gain values of 17.5 dB and 10 dB, respectively, at an outage probability value of 10^{-1}. In addition, the adaptive combining scheme with $\bar{\gamma}^r_{SD} = \bar{\gamma}^f_{SD}$ (i.e. average electrical SNR of FSO link varying equally with average SNR of RF link) performs better than the adaptive combining scheme with fixed RF average SNR scenario. In this case, the SNR gain value of 3 dB is obtained to achieve the outage value of 10^{-1}. Also, the performance of adaptive combining scheme deteriorates till $\bar{\gamma}^f_{SD} = 5$ dB for the case when $\bar{\gamma}^r_{SD} = \bar{\gamma}^f_{SD}$ compared to the case when $\bar{\gamma}^r_{SD} = 5$ dB due to degradation in the quality of RF link. However, the performance improves when $\bar{\gamma}^f_{SD} > 5$ dB, which is mainly due to the availability of better quality backup RF links.

In Fig. 5(a), we have also compared the outage performance of the single-hop RF system with the single-hop FSO and hybrid FSO/RF systems. It is inferred from the plots that the outage performance of RF system is better than the FSO system. This is due to the fact that the FSO link performance degrades mainly due to both atmospheric turbulence induced fading and pointing errors, where as the RF link performance degrades only due to small scale fading. Further, improvement in the outage performance of single-hop RF system is observed especially in the high-SNR region compared to hybrid FSO/RF system considering both hard-switching and adaptive combining schemes. This is because, as the average electrical SNR of FSO link increases, the probability that the RF link will be active in the high-SNR region in case of hybrid FSO/RF system is lesser compared to low-SNR region. Since FSO link will be active in most of the occasion in case of hybrid FSO/RF system in the high-SNR region, degradation in the outage performance of hybrid FSO/RF system compared to RF system is noticed as shown in Fig. 5(a).

In Fig. 5(b), the average SER performance comparison of all three system models (i.e. hard-switching, adaptive combining, and single-hop FSO) are shown for uplink scenario assuming both single-hop and dual-hop scenarios. Furthermore, from Fig. 5(b), we can observe that single-hop hybrid FSO/RF system with adaptive combining scheme performs better than single-hop FSO system with the SNR gain of around 16 dB at the SER value of 10^{-3} due to backup RF link. Similarly, dual-hop hybrid FSO/RF system with adaptive combining scheme performs better than dual-hop FSO system with the SNR gain of around 14 dB at the SER value of 10^{-3}. Thus, introducing HAPS reduces the SNR gain obtained by hybrid system over FSO system due to decoding errors. It is also observed that the hybrid FSO/RF system (both single-hop and dual-hop) with adaptive combining scheme performs better than the hard-switching-based hybrid FSO/RF system with the SNR gain of more than 6 dB at the SER value of 10^{-3} due to MRC of RF and FSO links at the receiver. Most importantly, it has been observed that the dual-hop FSO system performs better than the single-hop FSO system with the SNR gain of 4 dB at the SER value of 10^{-3}. This gain value is more than the SNR gain obtained by dual-hop hybrid system with both hard-switching and adaptive combining schemes compared to single-hop hybrid system as observed in the SER plots. Thus, it can be inferred that employing HAPS in a hybrid SATCOM system with both FSO and RF links reduces the SNR gain of the system.

Fig. 6(a) shows the effect of Ricean factor K on the outage probability of single-hop and dual-hop hybrid FSO/RF systems for the case of uplink scenario. From the plots,

This work is licensed under a Creative Commons Attribution 4.0 License. For more information, see https://creativecommons.org/licenses/by/4.0/

This article has been accepted for publication in a future issue of this journal, but has not been fully edited. Content may change prior to final publication. Citation information: DOI 10.1109/ACCESS.2021.3086024, IEEE Access

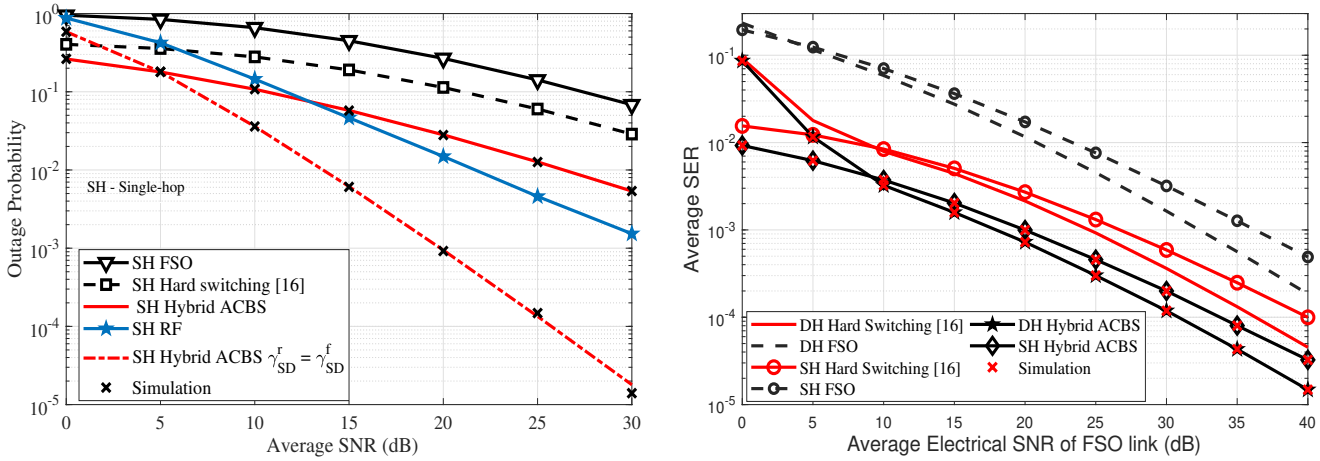

(a) Outage comparison of different switching schemes and system models

(b) SER comparison of different switching schemes and system models

FIGURE 5: Performance comparison of various system models and switching schemes for SATCOM system

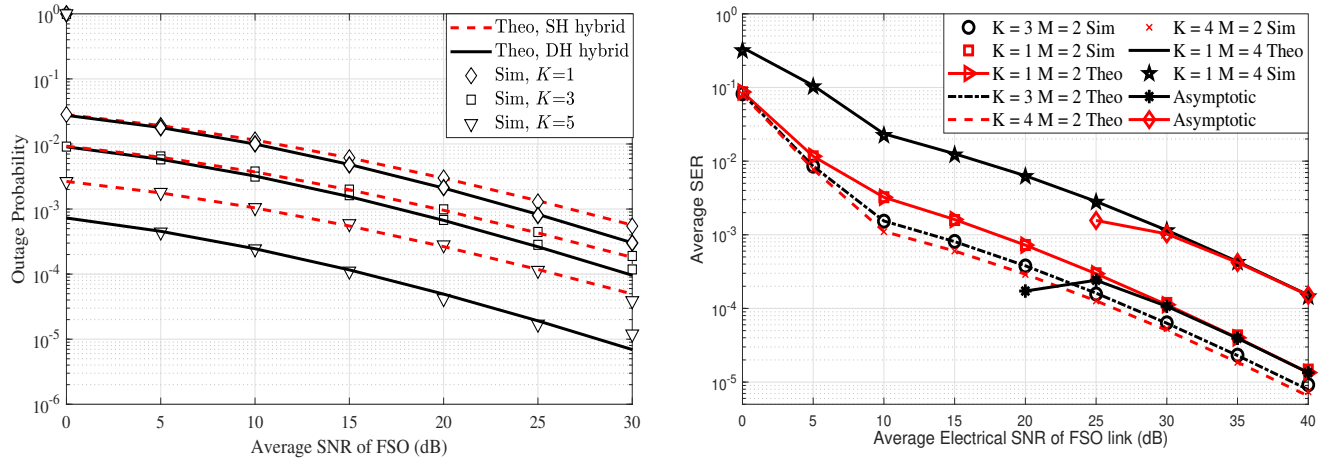

(a) Outage

(b) Average SER

FIGURE 6: System performance parameters vs Average electrical SNR of FSO link for varying K for uplink scenario

we can observe that with the increase in Ricean factor, the outage performance improves. We can achieve higher SNR gain from the outage performance of both the systems as K increases. Fig. 6(b) shows the effect of K on the average SER of dual-hop hybrid FSO/RF SATCOM system with adaptive combining scheme for the uplink scenario. Similar to outage performance, we can observe that with the increase in Ricean factor, the system performance increases. We can also observe improvement in the SNR gain of the hybrid system as K increases. So we can infer from both the figures that as K increases, the system performance increases. In addition, it is also observed from Fig. 6(b) that the asymptotic SER performance curves match with the exact average SER performance curves at high values of average electrical SNR of the FSO link. This also justifies that the derived asymptotic SER expressions are sufficiently tight with the exact SER expressions at high-SNR region. Further, it also validates the obtained diversity order of the proposed dual-hop hybrid FSO/RF SATCOM system as $\min\{\frac{\zeta_{SR}^2}{2}, \frac{\alpha_1^{up}}{2}, \frac{\beta_1^{up}}{2}\}$, which is equal to the diversity order of dual-hop FSO SATCOM system. This is because, if the average SNR of RF link and the optimum switching threshold SNR are fixed, then at high values of average electrical SNR of FSO link (i.e. $\bar{\gamma}_{SR}^{f} >> \gamma_T$), the probability that the instantaneous SNR of FSO link γ_{SR}^{f} falling below γ_T will be less. Hence, in case of adaptive-combining-based hybrid FSO/RF SATCOM system, only FSO link will be active in the high-SNR region, which will contribute to the diversity gain of the hybrid system. Kindly note that the derived asymptotic expressions are valid only in the high-SNR region. Thus, the asymptotic performance curves converge with the exact performance curves in the high-SNR region as shown in Fig. 6(b). Since the asymptotic expressions are derived under high-SNR approximations to calculate diversity gain, they are unpredictable and will not

This work is licensed under a Creative Commons Attribution 4.0 License. For more information, see https://creativecommons.org/licenses/by/4.0/

This article has been accepted for publication in a future issue of this journal, but has not been fully edited. Content may change prior to final publication. Citation information: DOI 10.1109/ACCESS.2021.3086024, IEEE Access

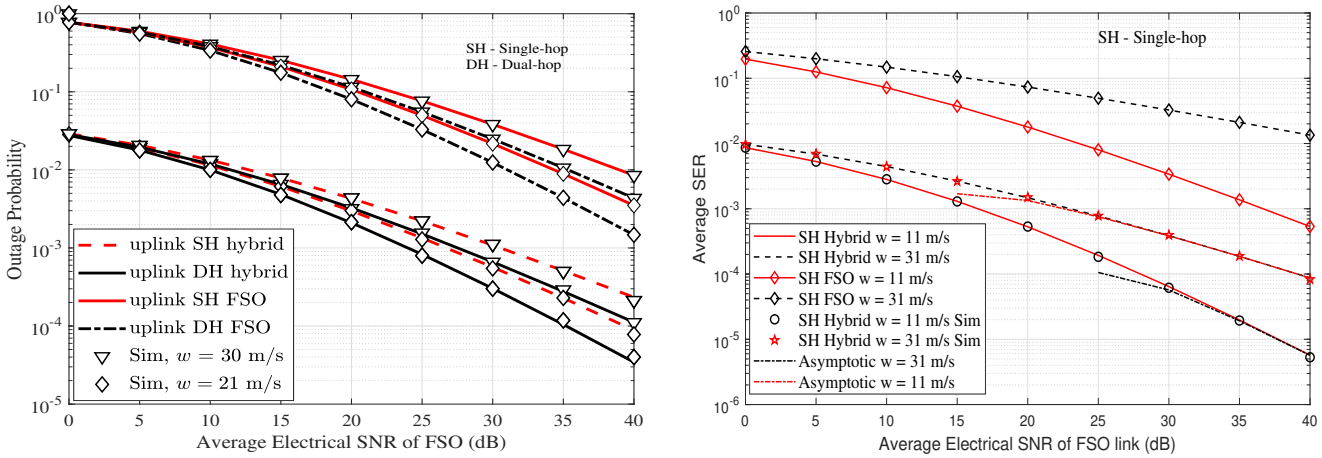

(a) Outage

(b) Average SER

FIGURE 7: System performance parameters vs Average electrical SNR of FSO link for different wind speed for uplink scenario

converge with the exact performance curves in the low-SNR region. This phenomenon will result in bending of the asymptotic curves in the low-SNR region in some occasion as shown in Fig. 6(b) as well as in other figures. Finally, it is observed that the derived analytical expressions for average SER and outage probability match exactly with the Monte-Carlo simulations in this figure and in all the other figures. Here, the average SER performance deteriorates with increase in modulation order M as expected.

In Fig. 7, the outage and average SER performances are shown for different wind speed values w for the case of uplink scenario. From Fig. 7(a), we can observe that with the increase in wind speed, the outage performance of the single-hop and dual-hop hybrid SATCOM systems deteriorate. This is because, the formation of vortexes in air increases as wind speed increases. This will effectively change the refractive index of the medium causing beam wander induced pointing errors and higher randomness in the received signal amplitude. This can cause degradation in the system performance, which is observed from the trends. Similar trends are observed in the case of average SER of the single-hop hybrid SATCOM system with adaptive combining scheme. From Fig. 7(b), we can see that as wind speed increases, the diversity order of the system decreases and hence, the average SER performance deteriorates to a larger extent at high-SNR region. On comparing the outage performance of the single-hop adaptive-combining-based hybrid system and single-hop FSO system, we obtain the SNR gains of approximately 27.5 dB and 24 dB at the wind velocity values of 30 m/s and 21 m/s, respectively, in favour of the hybrid system to achieve the outage value of 10^{-2}. Similarly, while comparing the average SER performance of single-hop adaptive-combining-based hybrid system and single-hop FSO system, we observe improvement in the SNR gain due to hybrid system for the wind velocity values of 30 m/s compared to 11 m/s. Thus, backup RF link helps in enhancing the performance for the worst case scenario with high wind velocity values. It is also noticed that the asymptotic SER values of single-hop hybrid system almost match the exact SER values in the high-SNR region, which validates the obtained diversity order of the system.

In Fig. 8, we plot the variation of system performance parameters for the uplink scenario with respect to varying zenith angle values. With increase in the zenith angle, the propagation distance of the FSO beam increases. This increases the divergence of the FSO beam, thus degrading the system performance. This trend can be observed from both Fig. 8(a) and 8(b). As zenith angle increases, it is also observed that the diversity order of both single-hop and dual-hop hybrid systems decreases. It is also inferred from the figure that increase in zenith angle value ϕ_z degrades the performance of both FSO and hybrid FSO/RF systems. This is because, the propagation distance of the optical signal increases with increase in ϕ_z. Hence, the transmitted optical beam will be more vulnerable to the atmospheric turbulence and pointing errors, which significantly degrades the performance and diversity order of the system. Most importantly, it is also observed that increase in ϕ_z impacts the performance of FSO system to a greater extent compared to hybrid FSO/RF system. Hence, reliable RF backup link has reduced the impact of increase in ϕ_z on the system performance.

The effect of pointing errors on the dual-hop FSO and hybrid FSO/RF systems is illustrated for an uplink scenario in Fig. 9 by varying the pointing error coefficient ξ_{SR}. The average SER performances are compared by assuming the parameters in the simulations as $\xi_{RD} = 6$, $\gamma_T = 5$ dB, and $\xi_{SR} = 1, 1.7$, and 5. To obtain the corresponding values of ξ_{SR}, mean and standard deviation values are, respectively, assumed as $\mu_x^{SR} = \mu_y^{SR} = 35$ cm, 0 cm, 1 cm, $\sigma_x^{SR} = \sigma_y^{SR} = 40$ cm, 30 cm, 10 cm. It is to be noted that the severity of pointing errors is low for higher values of ξ_{SR} and

This work is licensed under a Creative Commons Attribution 4.0 License. For more information, see https://creativecommons.org/licenses/by/4.0/

This article has been accepted for publication in a future issue of this journal, but has not been fully edited. Content may change prior to final publication. Citation information: DOI 10.1109/ACCESS.2021.3086024, IEEE Access

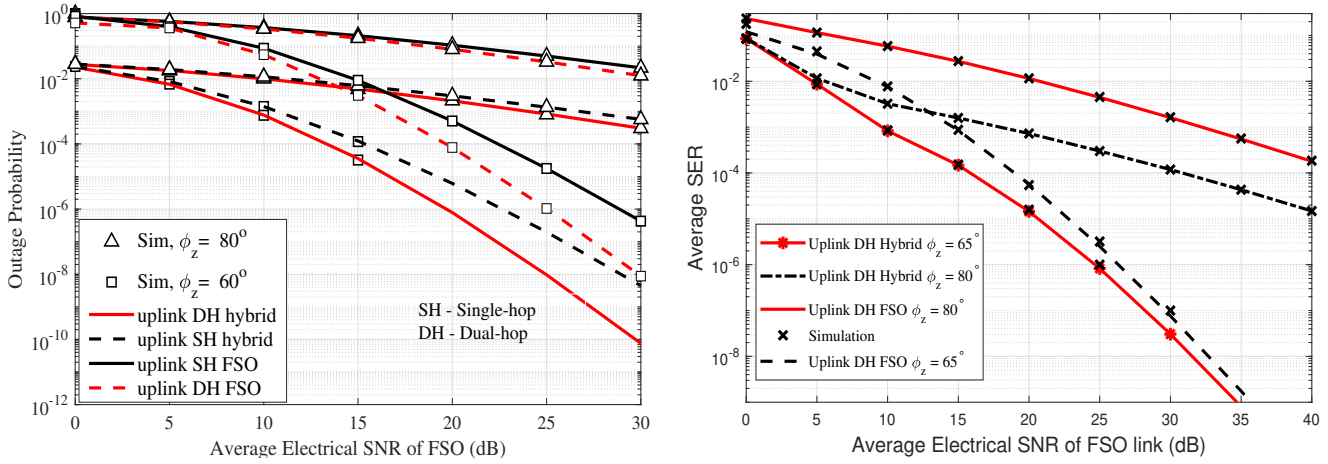

(a) Outage **(b)** Average SER

FIGURE 8: System performance parameters vs Average electrical SNR of FSO link for varying ϕ_z for uplink scenario

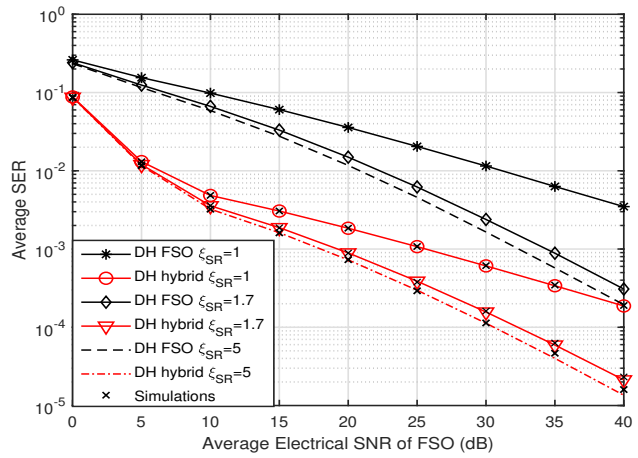

FIGURE 9: Average SER performance of dual-hop FSO and hybrid systems for different values of pointing error severity parameter ξ_{SR}

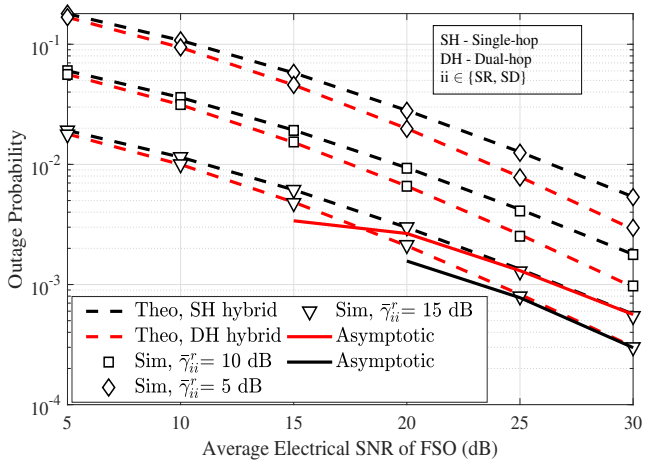

FIGURE 10: Outage probability vs Average electrical SNR of FSO link for different values of average SNR of RF for uplink scenario

we have assumed a high value of ξ_{RD} for HAPS-to-satellite FSO link, since the effect of pointing errors is very less or negligible. It is noticed from Fig. 9 that the SNR gain values achieved by the dual-hop hybrid FSO/RF system over dual-hop FSO system to attain the average SER of 10^{-2} are 24 dB, 17 dB, and 15 dB for $\xi_{SR} = 1, 1.7$, and 5, respectively. Therefore, it is clear that the dual-hop hybrid FSO/RF system with adaptive combining performs better than the dual-hop FSO system in all three cases and it provides high SNR gain due to the backup RF link when the severity of pointing errors is high. This is because of the fact that the probability of usage of backup RF link in case of adaptive combining increases with increase in severity of pointing errors, as the instantaneous SNR of FSO link often drops below γ_T.

Fig. 10 shows the outage performances of hybrid single-hop and dual-hop SATCOM systems for different values of average SNR of RF link. It is to be noted that increase in the value of average SNR of RF link indicates a better backup RF link, which directly translates to better system performance. As the value of RF average SNR increases, SNR gain improvement is observed in case of both the systems. Finally, it is also noticed that the outage values of single-hop and dual-hop hybrid systems almost match the exact values in the high-SNR region, which validates the obtained diversity order of the system.

VI. CONCLUSION AND FUTURE WORKS

In this paper, we analysed the performance of adaptive-combining-based switching scheme for uplink and downlink SATCOM scenarios assuming single-hop and dual-hop SAGIN-based hybrid FSO/RF systems. Further, we derived the exact and asymptotic outage and average SER expressions for both single-hop and dual-hop hybrid systems. From the asymptotic expressions, we obtained the diversity order

This work is licensed under a Creative Commons Attribution 4.0 License. For more information, see https://creativecommons.org/licenses/by/4.0/

This article has been accepted for publication in a future issue of this journal, but has not been fully edited. Content may change prior to final publication. Citation information: DOI 10.1109/ACCESS.2021.3086024, IEEE Access

$$\alpha_1^{up} = \left\{ 5.95(H_p - H_0)^2 sec^2(\phi_z) \left(\frac{2W_0}{r_0}\right)^{5/3} \left(\frac{\alpha_{pe}}{W}\right)^2 + \exp\left(\frac{0.49\sigma_R^2}{(1+0.56\sigma_R^{12/5})^{7/6}}\right) - 1 \right\}^{-1}, \quad (65)$$

of the proposed systems. From the numerical results, we inferred that the RF backup link in case of hybrid system is proved to provide a better system performance as compared to single-hop and dual-hop FSO systems. Moreover, we also obtained the optimum switching threshold value for the hybrid system. On comparing single-hop and dual-hop adaptive-combining-based hybrid FSO/RF systems, we conclude that dual-hop hybrid system provides a better system performance as compared to single-hop hybrid system only for the uplink scenario especially in the high-SNR region, while for the downlink scenario, the system performances are similar. Thus, the utilization of HAPS as a relay station improves the reliability of uplink SATCOM system in the high-SNR region. It was also observed that the adaptive-combining-based switching scheme performs better than the hard-switching scheme proposed for hybrid FSO/RF system. Finally, it was noticed that the SNR gain obtained due to single-hop and dual-hop hybrid systems compared to FSO system improves with increase in the values of Ricean factor, average SNR of RF link, zenith angle, severity of pointing errors, and wind speed.

The future work directions are given as follows: The ergodic capacity analysis of adaptive combining scheme along with the outage and average SER analyses will be carried out over generalized FSO and RF fading models assuming Malaga and $\alpha - \eta - \kappa - \mu$ distributions, respectively. In addition, the capacity bounds and asymptotic expressions for outage and average SER will be obtained over generalized distributions in order to get more insights in terms of achievable capacity and diversity gain. Finally, the switching time delay between RF and FSO links, which has been ignored in the current analysis, will also be considered in our future works.

.

APPENDIX A CALCULATION OF SMALL SCALE AND LARGE SCALE SCATTERING PARAMETERS

The single-hop uplink and downlink scattering parameters are calculated using [10], [11], and [24]. Furthermore, for GS-to-HAPS link, the large scale scattering parameter for dual-hop uplink scenario α_1^{up} is given by (65) and the small scale scattering parameter for dual-hop uplink scenario β_1^{up} is given as [10]

$$\beta_1^{up} = \left[\exp\left(\frac{0.51\sigma_R^2}{(1+0.69\sigma_R^{12/5})^{5/6}}\right) - 1 \right]^{-1}, \quad (66)$$

In (65) and (66), $(\sigma_R)^2$ is the Rytov variance and the same is given by (67), where $C_n^2(h)$ is the refractive index structure parameter, which is a function of altitude. It is modelled using HVB model [31] and is given by (68), where w is the rms wind speed and $C_n^2(0) = 1.7 \times 10^{-14}\text{m}^{-2/3}$. In (65) and (67), ϕ_z is the zenith angle, H_0 is the transmitter height in metre above the ground, H_p is the altitude of the HAPS in metre and $k = 2\pi/\lambda$ is the wave number in m^{-1}. In addition, W denotes the received beam size and is given by $W = W_0\sqrt{\Theta_0^2 + \Lambda_0^2}$, where W_0 is the beam size of transmitted beam, and Θ_0 and Λ_0 are the beam parameters at the transmitter. Note that $\Theta_0 = 1 - L_p/F_0$ and $\Lambda_0 = \frac{2L_p}{k(W_0)}$, where L_p is the propagation distance, which can be written as $L_p = (H_p - H_0) \times \sec(\phi_z)$ and F_0 is the phase front radius of curvature of the beam at the transmitter.

Furthermore, in (65), r_0 is the Fried parameter and α_{pe} is the beam-wander induced pointing error, which is given by $\alpha_{pe} = \sigma_{pe}/L_p$, where σ_{pe} is the variance of beam-wander induced pointing error and is calculated as

$$\sigma_{pe}^2 = 0.54(H_p - H_0)^2 \sec^2(\phi_z) \left(\frac{\lambda}{2W_0}\right)^2 \left(\frac{2W_0}{r_0}\right)^{5/3} \times \left[1 - \left(\frac{C_r^2 W_0^2/r_o^2}{1 + C_r^2 W_0^2/r_o^2}\right)^{1/6}\right], \quad (69)$$

where C_r is scaling constant and is assumed to be equal to 2π. The Fried parameter is calculated as

$$r_0 = \left[0.42 \sec(\phi_z)\, k^2 \int_{H_0}^{H_p} C_n^2(h) \mathrm{d}h\right]^{-3/5} \quad (70)$$

Similarly, to calculate α_2^{up} and β_2^{up}, we first calculate the Rytov variance and variance of beam-wander induced pointing error by substituting H_s, which is the height of LEO satellite, in place of H_p. In addition, H_p should be substituted in place of H_0. We use these values to calculate α_2^{up} and β_2^{up} similar to α_1^{up} and β_1^{up}, respectively.

Moreover, similar to the case of uplink scenario, the small scale and large scale scattering parameters of the downlink scenario are calculated by changing appropriate parameters using [12] and [16].

APPENDIX B ASYMPTOTIC OUTAGE PROBABILITY EXPRESSIONS

In this Appendix, various terms involved in asymptotic outage expressions are given below.

$$\mathcal{C}_1 = \sum_{k=1}^{6} \frac{\Gamma(\mathcal{B}_{8,k}) \prod_{\substack{j=1 \\ j\neq k}}^{6} \Gamma(\mathcal{B}_{8,j} - \mathcal{B}_{8,k})}{\Gamma(n+i+2+\mathcal{B}_{8,k}) \prod_{j=3}^{4} \Gamma(\mathcal{B}_{7,j} - \mathcal{B}_{8,k})} \times \left(\frac{D^2\gamma_{out}}{16}\right)^{\mathcal{B}_{8,k}} \quad (71)$$

$$\mathcal{C}_2 = \sum_{k=1}^{6} \frac{\prod_{\substack{j=1 \\ j\neq k}}^{6} \Gamma(\mathcal{B}_{4,j} - \mathcal{B}_{4,k})}{\mathcal{B}_{4,k} \prod_{j=2}^{3} \Gamma(\mathcal{B}_{3,j} - \mathcal{B}_{4,k})} \left(\frac{D^2\gamma_{out}}{16}\right)^{\mathcal{B}_{4,k}}, \quad (72)$$

This work is licensed under a Creative Commons Attribution 4.0 License. For more information, see https://creativecommons.org/licenses/by/4.0/

This article has been accepted for publication in a future issue of this journal, but has not been fully edited. Content may change prior to final publication. Citation information: DOI 10.1109/ACCESS.2021.3086024, IEEE Access

$$\sigma_R^2 = 2.25k^{7/6}(H_p - H_0)^{5/6}\sec^{11/6}(\phi_z)\int_{H_0}^{H_p} C_n^2(h) \times \left(1 - \frac{h - H_0}{H_p - H_0}\right)^{5/6}\left(\frac{h - H_0}{H_p - H_0}\right)^{5/6} \mathrm{d}h\,, \tag{67}$$

$$C_n^2(h) = 0.00594\left(\frac{w}{27}\right)^2 (10^{-5}h)^{10}\exp\left(\frac{-h}{1000}\right) + 2.7\times 10^{-16}\exp\left(\frac{-h}{1500}\right) + C_n^2(0)\exp\left(\frac{-h}{100}\right)\,, \tag{68}$$

$$\mathcal{C}_3 = \sum_{k=1}^{6} \frac{\prod_{\substack{j=1\\ j\neq k}}^{6}\Gamma(\mathcal{B}_{4,j} - \mathcal{B}_{4,k})}{\mathcal{B}_{4,k}\prod_{j=2}^{3}\Gamma(\mathcal{B}_{3,j} - \mathcal{B}_{4,k})}\left(\frac{D^2\gamma_T}{16}\right)^{\mathcal{B}_{4,k}}, \tag{73}$$

and

$$\mathcal{C}_4 = \sum_{k=1}^{6} \frac{\prod_{\substack{j=1\\ j\neq k}}^{6}\Gamma(\mathcal{B}_{10,j} - \mathcal{B}_{10,k})}{(p+\mathcal{B}_{10,k})\prod_{j=2}^{3}\Gamma(\mathcal{B}_{9,j} - \mathcal{B}_{10,k})}\left(\frac{D^2\gamma_T}{16}\right)^{\mathcal{B}_{10,k}}. \tag{74}$$

APPENDIX C DERIVATION OF ASYMPTOTIC SER EXPRESSIONS

In this section, we derive the asymptotic expressions for I_1 and I_2, which will help us in obtaining the asymptotic SER expressions for adaptive combining scheme in case of single-hop scenario.

From (34), (45) and [29, Eq. (07.34.06.0040.01)], we get the asymptotic expression for I_1 as

$$I_1^{asy} = \frac{A}{2}F_1^{asy}(\gamma_T) - \frac{2^{\alpha+\beta-3}\xi_{eq}^2 A F \gamma_T^{\frac{3}{2}} e^{-K}}{\pi^{\frac{3}{2}}\Gamma(\alpha)\Gamma(\beta)}\sum_{n=0}^{\infty}\frac{(-F\gamma_T)^n}{n!} \times \sum_{i=0}^{\infty}\frac{(KF\gamma_T)^i\Gamma(n+i+1)}{(i!)^2}\sum_{p=0}^{\infty}\frac{(-B\sqrt{\gamma_T})^{(2l+1)}}{l!(2l+1)}\mathcal{C}_5, \tag{75}$$

where

$$\mathcal{C}_5 = \sum_{k=1}^{6}\frac{\prod_{\substack{j=1\\ j\neq k}}^{6}\Gamma(\mathcal{B}_{14,j} - \mathcal{B}_{14,k})\prod_{j=1}^{2}\Gamma(1 - \mathcal{B}_{13,j} + \mathcal{B}_{14,k})}{\prod_{j=3}^{4}\Gamma(\mathcal{B}_{13,j} - \mathcal{B}_{14,k})\prod_{j=7}^{8}\Gamma(1 - \mathcal{B}_{14,j} + \mathcal{B}_{14,k})} \times \left(\frac{D^2\gamma_T}{16}\right)^{\mathcal{B}_{14,k}} \tag{76}$$

and the asymptotic expression for $F_1(\gamma_T)$ is given by

$$F_1^{asy}(\gamma_T) = \frac{2^{\alpha+\beta-3}\xi_{eq}^2 F e^{-K}}{\pi\Gamma(\alpha)\Gamma(\beta)}\sum_{n=0}^{\infty}\frac{(-F)^n}{n!}\sum_{i=0}^{\infty}\frac{(KF)^i}{(i!)^2} \times \gamma_T^{n+i+1}\Gamma(n+i+1)\,\mathcal{C}_6\,, \tag{77}$$

where

$$\mathcal{C}_6 = \sum_{k=1}^{6}\frac{\Gamma(\mathcal{B}_{8,k})\prod_{\substack{j=1\\ j\neq k}}^{6}\Gamma(\mathcal{B}_{8,j} - \mathcal{B}_{8,k})}{\Gamma(n+i+2+\mathcal{B}_{8,k})\prod_{j=3}^{4}\Gamma(\mathcal{B}_{7,j} - \mathcal{B}_{8,k})} \times \left(\frac{D^2\gamma_T}{16}\right)^{\mathcal{B}_{8,k}}. \tag{78}$$

On substituting (27) and (49) in (48), we get the asymptotic expression for I_2, which is given by

$$I_2^{asy} = H^{asy} - \frac{A}{2}F_{\gamma_{FSO}}^{asy}(\gamma_T) + I_{22}^{asy} + I_{23}^{asy} \tag{79}$$

Using (27), (49), (50), (51) and [29, Eq. (07.34.06.0040.01)], the terms in (79) can be written as

$$H^{asy} = \frac{2^{\alpha+\beta-4}A\xi_{eq}^2}{\pi^{3/2}\Gamma(\alpha)\Gamma(\beta)} \times \mathcal{C}_7, \tag{80}$$

$$F_{\gamma_{FSO}}^{asy}(\gamma_T) = \frac{2^{\alpha+\beta-3}\xi_{eq}^2}{\pi\Gamma(\alpha)\Gamma(\beta)} \times \mathcal{C}_3, \tag{81}$$

$$I_{22}^{asy} = \frac{2^{\alpha+\beta-3}\xi_{eq}^2 A}{\pi^{3/2}\Gamma(\alpha)\Gamma(\beta)}\sum_{n=0}^{\infty}\frac{(-1)^n(B\sqrt{\gamma_T})^{2n+1}}{n!(2n+1)} \times \mathcal{C}_8, \tag{82}$$

and

$$I_{23}^{asy} = \frac{2^{\alpha+\beta-4}\xi_{eq}^2 A F e^{-K}}{\pi^{\frac{3}{2}}\Gamma(\alpha)\Gamma(\beta)}\sum_{n=0}^{\infty}\frac{(-F)^n}{n!}\sum_{i=0}^{\infty}\frac{(KF)^i\gamma_T^{n+i+1}}{(i!)^2} \times \sum_{p=0}^{n+i}\binom{n+i}{l}(-1)^l G_{3,0}^{2,3}\left(B^2\gamma_T \,\middle|\, \begin{matrix}\mathcal{B}_{19}\\ \mathcal{B}_{20}\end{matrix}\right)\mathcal{C}_9, \tag{83}$$

where

$$\mathcal{C}_7 = \sum_{k=1}^{6}\frac{\Gamma(\frac{1}{2}+\mathcal{B}_{16,k})\prod_{\substack{j=1\\ j\neq k}}^{6}\Gamma(\mathcal{B}_{16,j} - \mathcal{B}_{16,k})}{\Gamma(\mathcal{B}_{16,k})\prod_{j=3}^{4}\Gamma(\mathcal{B}_{15,j} - \mathcal{B}_{16,k})}\left(\frac{D^2\gamma_T}{16}\right)^{\mathcal{B}_{16,k}}, \tag{84}$$

$$\mathcal{C}_8 = \sum_{k=1}^{6}\frac{\prod_{\substack{j=1\\ j\neq k}}^{6}\Gamma(\mathcal{B}_{18,j} - \mathcal{B}_{18,k})}{(n+\frac{1}{2}+\mathcal{B}_{18,k})\prod_{j=2}^{3}\Gamma(\mathcal{B}_{17,j} - \mathcal{B}_{18,k})} \times \left(\frac{D^2\gamma_T}{16}\right)^{\mathcal{B}_{18,k}}, \tag{85}$$

and

$$\mathcal{C}_9 = \sum_{k=1}^{6}\frac{\prod_{\substack{j=1\\ j\neq k}}^{6}\Gamma(\mathcal{B}_{12,j} - \mathcal{B}_{12,k})}{(l+\mathcal{B}_{12,k})\prod_{j=2}^{3}\Gamma(\mathcal{B}_{11,j} - \mathcal{B}_{12,k})}\left(\frac{D^2\gamma_T}{16}\right)^{\mathcal{B}_{12,k}}. \tag{86}$$

ACKNOWLEDGEMENT

This work is supported by the Start-up Research Grant (SRG) of Science and Engineering Research Board (SERB), Department of Science and Technology, Govt. of India and Singapore Ministry of Education Academic Research Fund Tier 1 grants.

This work is licensed under a Creative Commons Attribution 4.0 License. For more information, see https://creativecommons.org/licenses/by/4.0/

This article has been accepted for publication in a future issue of this journal, but has not been fully edited. Content may change prior to final publication. Citation information: DOI 10.1109/ACCESS.2021.3086024, IEEE Access

REFERENCES

[1] Dillow C., *The drone that may never have to land*, Aug. 2013. Accessed on: Feb. 1 2021 [Archived]. Available on: https://fortune.com/2013/08/23/the-drone-that-may-never-have-to-land/

[2] David Grace and Mihael Mohorcic, *Broadband communications via high-altitude platforms*, Wiley Telecom, 2011.

[3] J. Liu, Y. Shi, Z. M. Fadlullah, and N. Kato, "Space-air-ground integrated network: A survey," *IEEE Commun. Surveys & Tuts.*, vol. 20, no. 4, pp. 2714–2741, Fourthquarter 2018.

[4] M. A. Khalighi and M. Uysal, "Survey on free space optical communication: A communication theory perspective," *IEEE Commun. Surveys & Tuts.*, vol. 16, no. 4, pp. 2231-2258, Fourthquarter 2014.

[5] H. Kaushal and G. Kaddoum, "Optical communication in space: challenges and mitigation techniques," *IEEE Commun. Surveys & Tuts.*, vol. 19, no. 1, pp. 57-96, Firstquarter 2017.

[6] V. W. S. Chan, "Optical satellite networks," *J. Lightw. Technol.*, vol. 21, no. 11, pp. 2811-2827, Nov. 2003.

[7] T. Jono, Y. Takayama, K. Shiratama, I. Mase, B. Demelenne, Z. Sodnik, A. Bird, M. Toyoshima, H. Kunimori, D. Giggenbach, N. Perlot, M. Knapek, and K. Arai, "Overview of the inter-orbit and the orbit-to-ground laser communication demonstration by OICETS," *in Proc. SPIE*, San Jose, USA, 2007, pp. 1-10.

[8] H. Hemmati, A. Biswas, and I. B. Djordjevic, "Deep-space optical communications: Future perspectives and applications," *Proc. IEEE*, vol. 99, no. 11, pp. 2020-2039, Nov. 2011.

[9] J. Ma, K. Li, L. Tan, S. Yu, and Y. Cao, "Performance analysis of satellite-to-ground downlink coherent optical communications with spatial diversity over Gamma-Gamma atmospheric turbulence," *Appl. Opt.*, vol. 54, no. 25, pp. 7575-7585, Sep. 2015.

[10] A. Viswanath, V. K. Jain, and S. Kar, "Analysis of earth-to-satellite free-space optical link performance in the presence of turbulence, beam-wander induced pointing error and weather conditions for different intensity modulation schemes," *IET Commun.*, vol. 9, no. 18, pp. 2253-2258, Dec. 2015.

[11] A. Viswanath, P. Gopal, V. K. Jain, and S. Kar, "Performance enhancement by aperture averaging in terrestrial and satellite free space optical links," *IET Optoelectron.*, vol. 10, no. 3, pp. 111-117, May 2016.

[12] Minh Q. Vu, Nga T.T. Nguyen, Hien T.T. Pham, and Ngoc T. Dang, "Performance enhancement of LEO-to-ground FSO systems using All-optical HAP-based relaying," *Phys. Commun.*, vol. 31, pp. 218-229, Dec. 2018.

[13] F. Fidler, M. Knapek, J. Horwath, and W. R. Leeb, "Optical communications for high-altitude platforms," *IEEE J. Sel. Topics Quantum Electron.*, vol. 16, no. 5, pp. 1158-1070, Sep.-Oct. 2010.

[14] N. D. Chatzidiamantis, G. K. Karagiannidis, E. E. Kriezis, and M. Matthaiou, "Diversity combining in hybrid RF/FSO systems with PSK modulation," *in Proc. IEEE ICC*, Kyoto, 2011, pp. 1-6.

[15] M. Usman, H.-C. Yang, and M.-S. Alouini, "Practical switching-based hybrid FSO/RF transmission and its performance analysis," *IEEE Photon. J.*, vol. 6, no. 5, pp. 1–13, Oct. 2014.

[16] Swaminathan R, S. Sharma, N. Vishwakarma, and AS Madhukumar, "HAPS-based relaying for integrated space-air-ground networks with hybrid FSO/RF communication : A performance analysis," *IEEE Trans. Aerosp. Electron. Syst.*, Early Access, 2021, DoI: 10.1109/TAES.2021.3050663.

[17] T. Rakia, H. Yang, M. Alouini, and F. Gebali, "Outage analysis of practical FSO/RF hybrid system with adaptive combining," *IEEE Commun. Lett.*, vol. 19, no. 8, pp. 1366-1369, Aug. 2015.

[18] M. Siddharth, S. Suyash, and Swaminathan R, "Outage analysis of adaptive combining scheme for hybrid FSO/RF communication," *in Proc. IEEE National Conference on Communications (NCC)*, IIT Kharagpur, India, 2020, pp. 1-6.

[19] L. Yang, J. Yuan, X. Liu, and M. O. Hasna, "On the performance of LAP-based multiple-hop RF/FSO systems," *IEEE Trans. Aerosp. Electron. Syst.*, vol. 55, no. 1, pp. 499-505, Feb. 2019.

[20] E. Zedini, A. Kammoun, and M. Alouini, "Performance of multibeam very high throughput satellite systems based on FSO feeder links with HPA nonlinearity," *IEEE Trans. Wireless Commun.*, vol. 19, no. 9, pp. 5908-5923, Sep. 2020.

[21] G. Pan, J. Ye, Y. Zhang, and M. Alouini, "Performance analysis and optimization of cooperative satellite-aerial-terrestrial systems," *IEEE Trans. Wireless Commun.*, vol. 19, no. 10, pp. 6693-6707, Oct. 2020.

[22] H. Safi, A. Dargahi, J. Cheng, and M. Safari, "Analytical channel model and link design optimization for ground-to-HAP free-space optical communications," *J. Lightw. Technol.*, vol. 38, no. 18, pp. 5036-5047, Sep. 2020.

[23] M. Li, Y. Hong, C. Zeng, Y. Song, and X. Zhang, "Investigation on the UAV-to-satellite optical communication systems," *IEEE J. Sel. Areas Commun.*, vol. 36, no. 9, pp. 2128-2138, Sep. 2018.

[24] H. Kaushal, V. K. Jain, and S. Kar, *Free space optical communication*, Springer India, 2017.

[25] B. Ashrafzadeh, E. Soleimani-Nasab, M. Kamandar, and M. Uysal, "A framework on the performance analysis of dual-hop mixed FSO-RF cooperative systems," *IEEE Trans. on Commun.*, vol. 67, no. 7, pp. 4939-4954, July 2019.

[26] R. Boluda-Ruiz, A. García-Zambrana, C. Castillo-Vázquez, and B. Castillo-Vázquez, "Novel approximation of misalignment fading modeled by Beckmann distribution on free-space optical links," *Opt. Express*, vol. 24, no. 20, pp. 22635-22649, Oct. 2016.

[27] M. K. Simon and M.-S. Alouini, *Digital communications over fading channels: A unified approach to performance analysis*, 2nd ed. New York, NY, USA: Wiley-Interscience, 2005.

[28] I. S. Gradshteyn and I. M. Ryzhik, *Table of integrals, series, and products*, Elsevier Academic Press, USA, 2007.

[29] The Wolfram Research Meijer G-function document. [Online]. Available: https://functions.wolfram.com/PDF/MeijerG.pdf

[30] M. D. Selvaraj and R. K. Mallik, "Error analysis of the decode and forward protocol with selection combining," *IEEE Trans. Wireless Commun.*, vol. 8, no. 6, pp. 3086-3094, June 2009.

[31] Andrews, L.C., Phillips, and R.L., *Laser beam propagation through random media* SPIE Press, Washington, 2005

SUYASH SHAH is a pass out of Indian Institute of Technology (IIT) Indore 2020 batch. He got his Bachelor's degree in electrical engineering. His research interest involves design and analysis of hybrid free-space optics/radio frequency for terrestrial and satellite communication.

MOKKAPATI SIDDHARTH completed Bachelor of Technology in Electrical Engineering from IIT Indore in 2020. His research work includes performance analysis of hybrid free-space optics/radio frequency communication systems and that of nanowire junctionless transistors.

This work is licensed under a Creative Commons Attribution 4.0 License. For more information, see https://creativecommons.org/licenses/by/4.0/

This article has been accepted for publication in a future issue of this journal, but has not been fully edited. Content may change prior to final publication. Citation information: DOI 10.1109/ACCESS.2021.3086024, IEEE Access

NARENDRA VISHWAKARMA is currently pursuing his Ph.D degree with the Department of Electrical Engineering, Indian Institute of Technology (IIT) Indore. His current research interest focuses on the design and analysis of hybrid free space optics/radio frequency communication systems, performance analysis of wireless digital communication systems over generalized fading models, next-generation terrestrial and satellite communication systems, etc. Earlier, he received his B.E. degree in Electronics and Communication Engineering from RGPV Bhopal, India and M.Tech. degree in computer technology from IIT Delhi, India.

SWAMINATHAN R is currently working as an Assistant Professor in the Department of Electrical Engineering, IIT Indore. Earlier, he completed his PhD from IIT Kharagpur in 2016 and worked as a Post-doctoral Research Fellow at Nanyang Technological University (NTU) Singapore from 2016 to 2019. He received the B.Tech. degree in ECE from SASTRA University, Thanjavur, in 2009 and M.E. degree in communication systems from the College of Engineering Guindy, Anna University, Chennai, in 2011. His research interests include efficient design of Space-Air-Ground Integrated Networks (SAGIN) with hybrid optical-RF wireless communications, Unmanned-Aerial-Vehicle (UAV)-assisted Free Space Optics (FSO) communication, Development of novel algorithms for blind parameter estimation of forward error correcting codes and interleavers, Beyond 5G and 6G wireless systems, Index modulation techniques for next-generation wireless communications, Energy harvesting schemes for integrated optical-RF networks, Non-Orthogonal Multiple Access (NOMA) techniques, Intelligent-Reflecting-Surfaces (IRS)-aided wireless communications, etc. Dr. Swaminathan received the gold medal from the College of Engineering Guindy, Anna University. He is the author or co-author of 20 International journal publications including 13 publications in reputed IEEE Journals/Transactions/Letters. Furthermore, he has been serving as a Reviewer for reputed IEEE journals and as a TPC member for reputed IEEE conferences.

AS MADHUKUMAR'S expertise lies in the areas of multi-tier cellular architecture, cooperative and cognitive radio systems, interference management, coding and modulation, new multiple access schemes, hybrid radio systems and other advanced signal processing algorithms for future communication systems. He is involved in a number of funded research projects, organizing international conferences, and a permanent reviewer for many internationally reputed journals and conferences. He has published over 300 referred international conference and journal papers. He is a recipient of Nanyang Award for Teaching Excellence in 2007 and obtained best paper awards in IEEE 35th Digital Avionics Conference in 2016 and in IEEE Integrated Communications, Navigations and Surveillance Conference in 2016 and in 2017.

AS Madhukumar received his B Tech degree from College of Engineering, Trivandrum, India, M Tech from Cochin University of Science and Technology, India and PhD from Department of Computer Science and Engineering, Indian Institute of Technology, Madras, India. He is currently an Associate Professor in the School of Computer Engineering, Nanyang Technological University, Singapore. Before joining NTU, he was involved in communications and signal processing research at Centre for Development of Advanced Computing (Electronics R&D Centre), Govt. of India and Institute for Infocomm Research (Centre for Wireless Communications), Singapore. Dr. Madhukumar is a senior member of IEEE.

This work is licensed under a Creative Commons Attribution 4.0 License. For more information, see https://creativecommons.org/licenses/by/4.0/